SUPPORTING INFORMATION

Direct Synthesis of Doubly Deprotonated, Dearomatised Lutidine PNP Cr and Zr Pincer Complexes Based on Isolated K and Li Ligand Transfer Reagents

Thomas Simler,[a] Gilles Frison,[b] Pierre Braunstein*[a] and Andreas A. Danopoulos*[ac]

[a.] *Laboratoire de Chimie de Coordination, Institut de Chimie (UMR 7177 CNRS), Université de Strasbourg, France*

[b.] *LCM, CNRS, Ecole polytechnique, Université Paris-Saclay, 91128 Palaiseau, France*

[c.] *Institute for Advanced Study (USIAS), Université de Strasbourg, France*

E-mail: braunstein@unistra.fr*,* danopoulos@unistra.fr

Contents

I. SYNTHESIS AND CHARACTERISATION

I.1. General considerations

All air- and moisture-sensitive manipulations were performed under dry argon atmosphere using standard Schlenk techniques or in an MBraun glove-box containing an atmosphere of N$_2$. THF and Et$_2$O were dried by refluxing over sodium/benzophenone ketyl and distilled under an argon atmosphere prior use. Pentane and toluene were dried by passing through columns of activated alumina and subsequently purged with argon. C$_6$D$_6$ and THF-d_8 were distilled over KH and were degassed by freeze-pump-thaw cycles. [CrCl$_2$(THF)$_2$] was prepared by continuous extraction of commercial anhydrous CrCl$_2$ (Aldrich) into dry THF for 3 days, followed by evaporation of the volatiles from the suspension of the extracted complex and drying the light green-gray residue under vacuum for *ca.* 20 min. Benzyl potassium (KBn),[1] [ZrCl$_4$(THT)$_2$][2] (THT = tetrahydrothiophene) and 2,6-bis-(di-*tert*-butylphosphinomethyl)-pyridine (^{tBu}PN^{tBu}P) were prepared according to literature procedures.[3] Solid LiCH$_2$SiMe$_3$ was obtained from commercial solutions (Aldrich) by evaporation of the pentane under vacuum. All other chemicals, from commercial sources, were used without further purification.

NMR spectra were recorded on Bruker spectrometers (AVANCE I – 300 MHz, AVANCE III – 400 MHz, AVANCE III – 600 MHz or AVANCE I – 500 MHz equipped with a cryogenic probe). Downfield shifts are reported in ppm as positive and referenced using signals of the residual protio solvent (^{1}H), the solvent (^{13}C) or externally (^{31}P, [7]Li). All NMR spectra were measured at 298 K, unless otherwise specified. The multiplicity of the signals is indicated as s = singlet, d = doublet, t = triplet, q = quartet, m = multiplet and br = broad. Assignments were determined on the basis of unambiguous chemical shifts and ^{13}C-DEPT experiments or 2D correlations (^{1}H-^{1}H COSY, ^{1}H-^{13}C HSQC, ^{1}H-^{13}C HMBC).

### I.2.   Synthetic procedure for the ᵗᴮᵘPNᵗᴮᵘP ligand
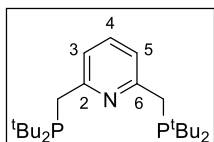
2,6-Bis-(di-*tert*-butylphosphinomethyl)-pyridine ($^{tBu}PN^{tBu}P$) was synthesised according to the literature procedure,[3] starting from 2,6-lutidine (1.48 g, 13.8 mmol), ^{n}BuLi (17.7 mL of a 1.6 M hexane solution, 28.3 mmol) and di-*tert*-butylchlorophosphine (4.99 g, 27.6 mmol). Yield after recrystallisation: 2.85 g (7.21 mmol), 52%.

^{1}H NMR (400.13 MHz, C$_6$D$_6$): δ 7.24 (d, $^{3}J_{HH}$ = 7.6 Hz, 2H, C$H_{pyr.}$ H^{3} + H^{5}), 7.16 (t, $^{3}J_{HH}$ = 7.6 Hz, 1H, C$H_{pyr.}$ H^{4}), 3.09 (d, $^{2}J_{PH}$ = 2.8 Hz, 4H, CH_2P), 1.12 (d, $^{3}J_{PH}$ = 10.7 Hz, 36H, C(CH_3)$_3$).

^{31}P{^{1}H} NMR (161.98 MHz, C$_6$D$_6$): δ 35.2 (s).

I.3.   Synthetic procedure for doubly deprotonated M$_2$(^{tBu}P*N$_a$^{tBu}P*)

I.3.1. Synthesis of K$_2$(^{tBu}P*N$_a$^{tBu}P*)
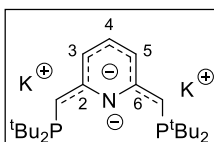
To a stirred solution of $^{tBu}PN^{tBu}P$ (0.791 g, 2.00 mmol) in toluene (10 mL) precooled at -78 °C was added KBn (0.521 g, 4.00 mmol). The resulting red solution was allowed to reach r.t. and a yellow precipitate appeared immediately. The solution was stirred overnight and the solid was filtered, rinsed with toluene (5 mL) and pentane (10 mL) and dried under vacuum for several hours to afford a yellow free-flowing powder of K$_2$(^{tBu}P*N$_a$^{tBu}P*)·0.6 toluene (toluene adduct based on the ^{1}H NMR spectrum in THF-d_8). Yield: 0.950 g (1.83 mmol), 92%. Satisfactory elemental analysis data could not be obtained, due to the *extreme* air sensitivity of the complex but its purity can be assessed from the NMR spectra (see Section IV).

The ^{1}H and ^{31}P{^{1}H} NMR data in THF-d_8 support the presence of a mixture of isomers due to Z→E isomerisation of the exocyclic partial double bonds in donor solvents (*cf.* section I.3.2), similarly to the phenomenon described for the related K(^{tBu}P*N$_a$C^{NHC}) complex.[4]

^{1}H NMR (400.13 MHz, THF-d_8): δ 7.22-7.04 (m, 2-3H, C$H_{toluene}$), 6.08-5.82 (m, 1.1H, C$H_{pyr.}$ H^{4}), 5.60-5.20 (m, 0.9H, H^{3}/H^{5}), 4.84-4.52 (m, 1.2H, H^{3}/H^{5}), 2.78-2.46 (m, 2H, CHP), 2.30 (s, 1.8H, C$H_{3\ toluene}$), 1.05 (br d, $^{3}J_{PH}$ = 10.0 Hz, 36H, C(CH_3)$_3$). ^{31}P{^{1}H} NMR (161.98 MHz, THF-d_8): δ 18.6 (s), 18.5 (overlapping s), 17.1 (br s), 15.9 (br s). ^{13}C{^{1}H} NMR (125.77 MHz, THF-d_8): δ 170.1 (br d, $^{2}J_{PC}$ = 33.9 Hz, $C_{pyr.}$), 138.2 ($C_{toluene}$), 132.6 (br, C$H_{pyr.}$), 129.5 (C$H_{toluene}$), 128.7 (C$H_{toluene}$), 125.8 (C$H_{toluene}$), 93.3 (br, C$H_{pyr.}$), 89.2 (br, C$H_{pyr.}$), 53.8-52.3 (m, CHP), 33.2-32.6 (m, C(CH_3)), 31.2-30.7 (m, C(CH_3)).

After evaporation and redissolution in C$_6$D$_6$, only one isomer was observed, consistent with the published results on the related K(^{tBu}P*N$_a$C^{NHC}) complex.[4]

^{1}H NMR (400.13 MHz, C$_6$D$_6$): δ 6.38 (br s, 1H, C$H_{pyr.}$ H^{4}), 4.99 (br s, 2H, C$H_{pyr.}$ H^{3} + H^{5}), 3.00 (br s, 2H, CHP), 1.30 (br d, $^{3}J_{PH}$ = 10.1 Hz, 36H, C(CH_3)$_3$). ^{31}P{^{1}H} NMR (161.98 MHz, C$_6$D$_6$): δ 13.1 (s). No ^{13}C{^{1}H} NMR spectrum could be recorded in C$_6$D$_6$ due to very poor solubility.

Noteworthy, K$_2$(^{tBu}P*N$_a$^{tBu}P*) slowly reacts with THF at room temperature to give *ca.* 6-7% of the mono-reprotonation product after standing in the NMR tube for 12 days. No decomposition in the solid state occurred when the compound was stored in the glovebox at room temperature.

I.3.2. Study of the structure of $K_2(^{tBu}P^*N_a^{tBu}P^*)$ in THF-d_8 solution

In order to prove the presence of different isomers in equilibrium in THF-d_8 solution, a ^{1}H-^{1}H NOESY experiment was carried out (see Scheme S1 and Figure S1).
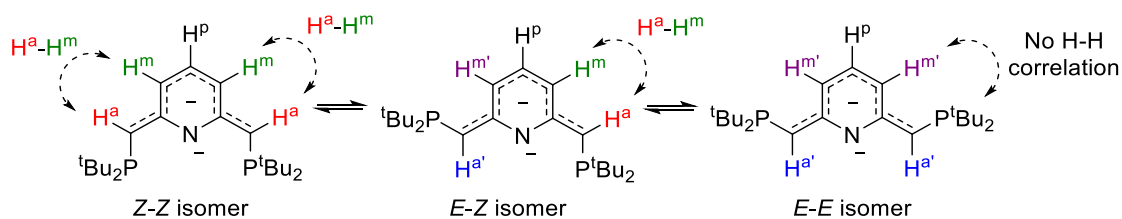
Scheme S1. The different isomers considered and assignment of the protons. Only the Z-isomers give rise to notable ^{1}H-^{1}H NOESY correlation with the vinylic H^a proton.
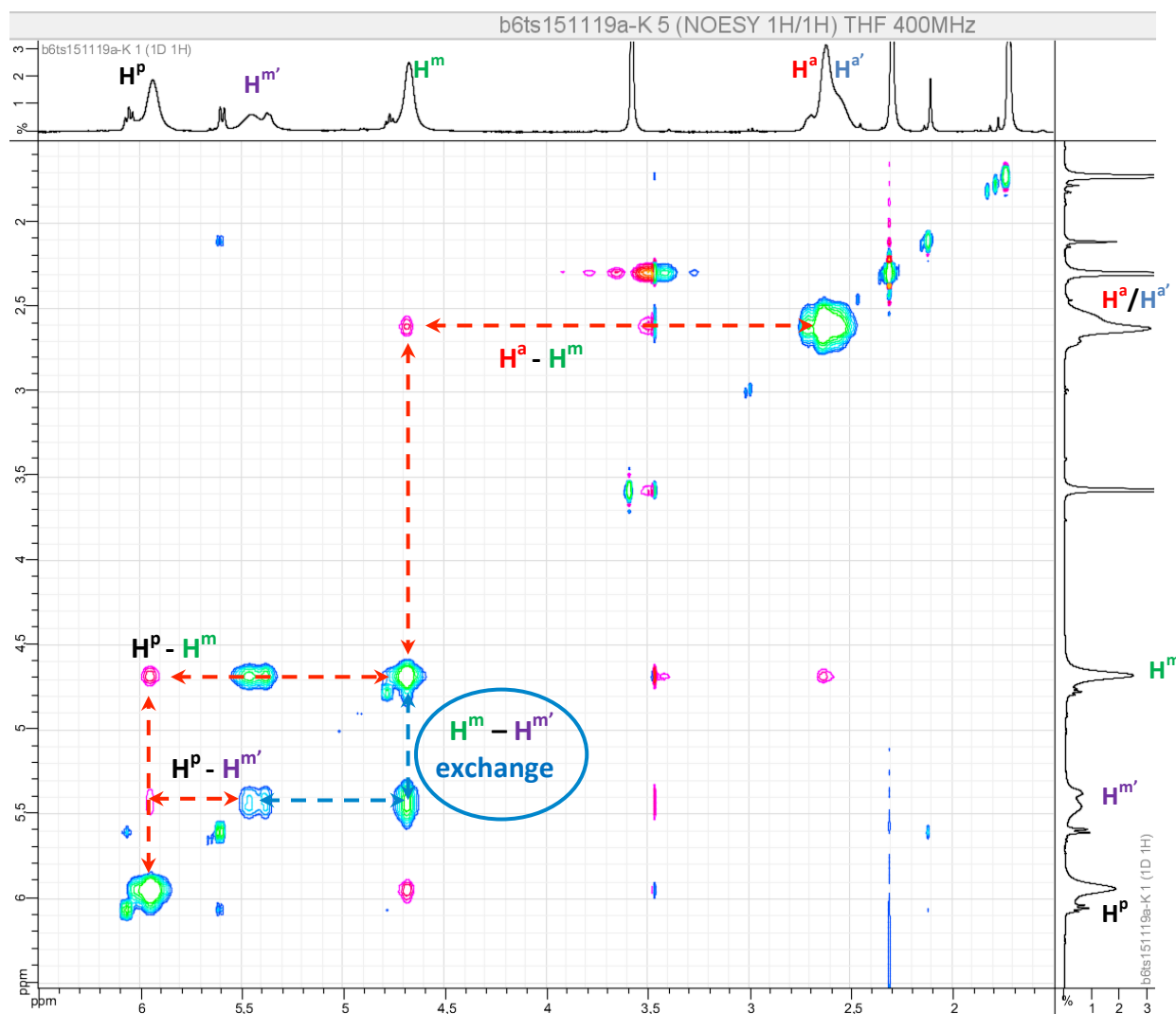

Figure S1. Representative NOESY spectrum of $K_2(^{tBu}P^*N_a^{tBu}P^*)$ in THF-d_8 showing the exchange between Z- and E-isomers (tentative assignment of the protons). The cross-correlations in blue present the same phase as the diagonal and correspond to exchange (EXSY) peaks while the correlations in red are due to through-space interaction (mixing time set at $\tau_m = 0.80$ s). H$^{m'}$ was identified due to the absence of through-space correlation with H$^{a'}$. Exchange between H^m and H$^{m'}$ confirms the dynamic equilibrium between the different isomers.

I.3.3. Synthesis of [Li$_2$(^{tBu}P*N$_a^{tBu}$P*)]$_2$ (1)
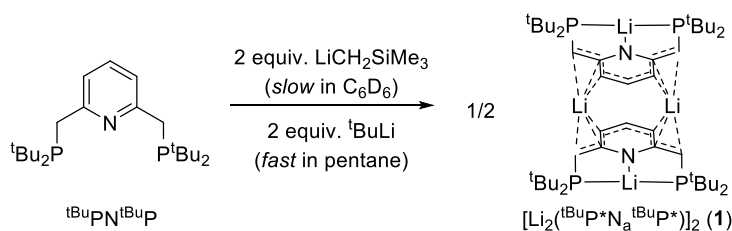
Scheme S2. Double deprotonation of ^{tBu}PN^{tBu}P with alkyllithium bases to afford **1**.
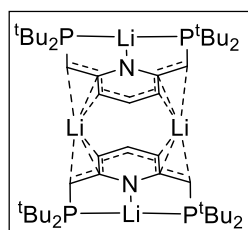
To a C$_6$D$_6$ solution of ^{tBu}PN^{tBu}P in a Young's NMR tube was added excess LiCH$_2$SiMe$_3$. The solution immediately turned orange and was heated to 50 °C. After several days of heating, orange-yellow crystals suitable for X-ray crystallography studies were obtained in the tube.

Interestingly, in an NMR experiment, the isolated compound **1** was mixed with excess SiMe$_4$ but no re-protonation of **1** was observed within one day. The sluggish formation of **1** by reaction of ^{tBu}PN^{tBu}P with LiCH$_2$SiMe$_3$ may thus originate from kinetic rather than thermodynamic reasons (pK_a difference between the conjugated acids).

[Li$_2$(^{tBu}P*N$_a^{tBu}$P*)]$_2$ can be prepared more efficiently on a 1-2 g scale using the following procedure:

In a Schlenk flask, ^{t}BuLi (6.5 mL of a 1.7 M hexane solution, 11.0 mmol) was slowly added at 0 °C to a stirred suspension of ^{tBu}PN^{tBu}P (1.98 g, 5.00 mmol) in pentane (10 mL). A yellow precipitate progressively appeared in the red solution and the reaction mixture was allowed to reach room temperature. After further stirring for 2 h, the Schlenk flask was transferred in the glovebox and the solid was filtered over a glass frit, rinsed with pentane (10 mL) and dried under vacuum to afford [Li$_2$(^{tBu}P*N$_a^{tBu}$P*)]$_2$ as a yellow free-flowing powder. Yield: 1.55 g (3.80 mmol), 76% based on the ligand. Satisfactory elemental analysis data could not be obtained, due to the *extreme* air sensitivity of the complex but its purity can be assessed from the NMR spectra (see Section IV).

^{1}H NMR (400.13 MHz, C$_6$D$_6$): δ 6.63 (t, $^3J_{HH}$ = 7.7 Hz, 1H, C$H_{pyr.}$ H^4), 5.41 (d, $^3J_{HH}$ = 7.7 Hz, 2H, C$H_{pyr.}$ H^3 + H^5), 2.84 (d, $^2J_{PH}$ = 9.3 Hz, 2H, CHP), 1.19 (d, $^3J_{PH}$ = 12.1 Hz, 36H, C(CH_3)$_3$).

^{13}C{^{1}H} NMR (125.77 MHz, C$_6$D$_6$): δ 172.0 (d, $^2J_{PC}$ = 17.2 Hz, $C_{pyr.}$ C^2 + C^6), 138.7 (C$H_{pyr.}$ C^4), 97.6 (m, C$H_{pyr.}$ C^3 + C^5), 49.3 (br s, CHP), 30.3 (br d, J_{PC} = 9.8 Hz, C(CH_3)). C(CH$_3$)$_3$ not observed (possibly masked by the peak at δ 30.3)

^{31}P{^{1}H} NMR (161.98 MHz, C$_6$D$_6$): δ 23.8 (br q, $^1J_{PLi}$ ≈ 70 Hz).

^{7}Li NMR (155.50 MHz, C$_6$D$_6$): δ 3.9 (br t, $^1J_{PLi}$ ≈ 70 Hz), 1.2 (br s).
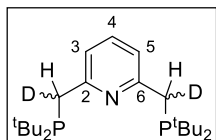
**Synthesis of 2,6-bis-(di-*tert*-butylphosphinomethyl-*d*)-pyridine**

To a THF-d_8 (resp. C_6D_6) solution of $K_2(^{tBu}P*N_a{}^{tBu}P*)\cdot0.6$toluene (resp. [Li$_2$(^{tBu}P*N$_a{}^{tBu}$P*)]$_2$) was added one drop of degassed D_2O under argon. A minor product was detected, which contains PCH$_2$ group(s). The chemical shift of the ^{31}P{^{1}H} signal, the integration of the α-C*H*DP protons and the multiplicity of the α-*C*HDP in the ^{13}C{^{1}H}/DEPT-NMR spectra all support formation of α,α'-d_2-^{tBu}PN^{tBu}P.

^{1}H NMR (500.13 MHz, THF-d_8): δ 7.45 (t, $^3J_{HH}$ = 7.7 Hz, 1H, C*H*$_{pyr.}$ H^4), 7.16 (d, $^3J_{HH}$ = 7.8 Hz, 2H, C*H*$_{pyr.}$ H^3 + H^5), 7.21-7.04 (overlapping m, residual C*H*$_{toluene}$, 3.3H), 2.98 (d, $^2J_{PH}$ = 2.9 Hz, 0.3H, minor species with C*H$_2$*P), 2.96 (br d, $^2J_{PH}$ = 1.8 Hz, 1.7H, C*H*DP), 2.29 (s, residual C*H$_3$* $_{toluene}$, 2H), 1.108 (d, $^3J_{PH}$ = 10.7 Hz, 18H, C(C*H$_3$*)$_3$), 1.106 (d, $^3J_{PH}$ = 10.7 Hz, 18H, C(C*H$_3$*)$_3$). ^{31}P{^{1}H} NMR (161.98 MHz, THF-d_8): δ 35.1 (s). ^{13}C{^{1}H} NMR (125.77 MHz, THF-d_8): δ 161.6 (d, $^2J_{PC}$ = 14.6 Hz, $C_{pyr.}$ C^2 + C^6), 138.2 (residual $C_{toluene}$), 136.2 (C*H*$_{pyr.}$ C^4), 129.4 (residual C*H*$_{toluene}$), 128.7 (residual C*H*$_{toluene}$), 125.8 (residual C*H*$_{toluene}$), 121.0 (dd, $^3J_{PC}$ = 9.8 Hz, $^5J_{PC}$ = 1.5 Hz, C*H*$_{pyr.}$ C^3 + C^5), 32.11 (d, $^1J_{PC}$ = 23.8 Hz, diastereotopic *C*(CH$_3$)$_3$), 32.08 (d, $^1J_{PC}$ = 23.8 Hz, diastereotopic *C*(CH$_3$)$_3$), 32.0 (overlapping d, $^2J_{PH}$ = 25.4 Hz, minor species with CH$_2$P), 31.8 (dt, $^1J_{PC}$ = 25.1 Hz, $^1J_{CD}$ = 19.6 Hz, *C*HDP), 29.9 (d, $^2J_{PC}$ = 13.9 Hz, C(*C*H$_3$)$_3$), 21.3 (residual *C*H$_3$ $_{toluene}$) (assignment of ^{13}C{^{1}H} NMR signals was confirmed by ^{13}C DEPT).

^{1}H NMR (400.13 MHz, C_6D_6): δ 7.24 (d, $^3J_{HH}$ = 7.6 Hz, 2H, C*H*$_{pyr.}$ H^3 + H^5), 7.16 (t, $^3J_{HH}$ = 7.6 Hz, 1H, C*H*$_{pyr.}$ H^4), 3.09 (d, $^2J_{PH}$ = 2.8 Hz, 0.3H, minor species with C*H$_2$*P), 3.07 (br d, $^2J_{PH}$ = 2.2 Hz, 1.7H, C*H*DP), 1.12 (2 overlapping d, $^3J_{PH}$ = 10.7 Hz, 36H, C(C*H$_3$*)$_3$). ^{31}P{^{1}H} NMR (161.98 MHz, C_6D_6): δ 35.0 (s). ^{13}C{^{1}H} NMR (125.77 MHz, C_6D_6): δ 161.6 (d, $^2J_{PC}$ = 14.6 Hz, $C_{pyr.}$ C^2 + C^6), 135.9 (C*H*$_{pyr.}$ C^4), 120.9 (dd, $^3J_{PC}$ = 9.7 Hz, $^5J_{PC}$ = 1.4 Hz, C*H*$_{pyr.}$ C^3 + C^5), 32.08 (dt, $^1J_{PC}$ = 25.0 Hz, $^1J_{CD}$ = 19.5 Hz, *C*HDP), 31.90 (d, $^1J_{PC}$ = 23.9 Hz, diastereotopic *C*(CH$_3$)$_3$), 31.88 (d, $^1J_{PC}$ = 23.9 Hz, diastereotopic *C*(CH$_3$)$_3$), 29.9 (d, $^2J_{PC}$ = 13.8 Hz, C(*C*H$_3$)$_3$) (assignment of ^{13}C{^{1}H} NMR signals was confirmed by ^{13}C DEPT).

I.5.   Transmetallation from [Li$_2$(^{tBu}P*N$_a{}^{tBu}$P*)]$_2$ to [Cr{Cr(^{tBu}P*N$_a{}^{tBu}$P*)Cl}$_2$] (2)

I.5.1.   Synthetic procedure
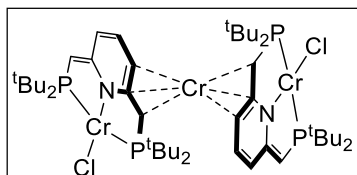
To a suspension of [CrCl$_2$(THF)$_2$] (0.057 g, 0.21 mmol) in THF (5 mL) precooled at −78 °C was added a solution of [Li$_2$(^{tBu}P*N$_a{}^{tBu}$P*)]$_2$ (0.087 g, 0.11 mmol) in THF (10 mL). The resulting dark-red brown solution was allowed to reach room temperature and was stirred for 1 h. The volatiles were evaporated under reduced pressure and the solid residue was extracted with a pentane and toluene and filtered. Slow evaporation of a concentrated pentane/Et$_2$O solution gave dark brown-red crystals of [Cr{Cr(^{tBu}P*N$_a{}^{tBu}$P*)Cl}$_2$]. Yield of the crystals: 0.023 g (0.023 mmol), 21%. Satisfactory elemental analysis data could not be obtained, due to the high air sensitivity of the

complex but its purity can be assessed from the NMR spectra (see Section IV). ^{1}H NMR (400.13 MHz, THF-d_8): characteristic signals at δ 94.9, 78.3, 63.7, -11.9, -20.9, -33.8, -79.6, -115.1. Precise assignment and integration is hampered by the presence of pentane in the asymmetric unit of the crystals (*cf.* section II.1), and by the overlap of the signals from the residual protio solvent present in THF-d_8 with the signals of **2**. Moreover, the crystal structure corresponds to one specific diastereoisomer; in solution different diasteroisomers may coexist leading to different signals.

I.5.2. Determination of the magnetic susceptibility

The determination of the magnetic susceptibility was carried out using Evans' method[5] for a THF-d_8 solution of **2** containing toluene as internal reference and using a capillary of toluene as a diamagnetic standard. The solvent correction was not applied[6] and the diamagnetic corrections were calculated using Pascal's constants.[7] The ^{1}H-NMR spectrum was recorded at 400.13 MHz and 298 K. μ_{eff} = 8.5(1) μ_B. This magnetic moment appears consistent with three uncoupled Cr(II) (d^4, S=2) centres, giving rise to a spin-only moment of $\mu_{eff} = \sqrt{3}$ x 4.90 μ_B = 8.49 μ_B.

I.6.   Transmetallation from [Li$_2$(^{tBu}P*N$_a$^{tBu}P*)]$_2$ to [Zr(^{tBu}P*N$_a$^{tBu}P*)Cl$_2$] (3)

I.6.1. Synthetic procedure
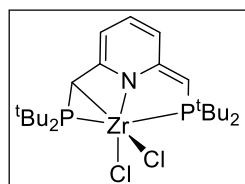
To a suspension of [ZrCl$_4$(THT)$_2$] (0.164 g, 0.40 mmol) in toluene (5 mL) precooled at −78 °C was added a solution of [Li$_2$(^{tBu}P*N$_a$^{tBu}P*)]$_2$ (0.163 g, 0.20 mmol) in toluene (10 mL). The resulting mixture immediately turned dark green and was stirred at r.t. for 1 h. All volatiles were removed under reduced pressure and the resulting solid was extracted with pentane. Filtration and slow evaporation of the solution in the glovebox at r.t. afforded dark-green crystals of [Zr(^{tBu}P*N$_a$^{tBu}P*)Cl$_2$]. Yield of the crystals: 0.160 g (0.29 mmol), 72%.

Anal. Calcd for C$_{23}$H$_{41}$Cl$_2$NP$_2$Zr (555.66): C, 49.72; H, 7.44; N, 2.52. Found: C, 49.33; H, 7.52; N, 2.39.

^{1}H NMR (400.13 MHz, C$_6$D$_6$, **298 K**): δ 6.50 (tt, $^3J_{HH}$ = 7.8 Hz, $^5J_{PH}$ = 1.3 Hz, 1H, C$H_{pyr.}$ H^4), 6.10 (br s, 1H, C$H_{pyr.}$ H^3/H^5), 5.20 (br s, 1H, C$H_{pyr.}$ H^5/H^3), 3.69 (br s, 1H, CHP), 2.28 (br s, 1H, CHP), 1.30 (br d, $^3J_{PH}$ = 12.7 Hz, 18H, C(CH_3)$_3$), 1.14 (br d, $^3J_{PH}$ = 12.3 Hz, 9H, C(CH_3)$_3$), 1.02 (br d, $^3J_{PH}$ = 13.6 Hz, 9H, C(CH_3)$_3$).

^{1}H NMR (400.13 MHz, C$_6$D$_6$, **343 K**): δ 6.46 (t, $^3J_{HH}$ = 7.8 Hz, 1H, C$H_{pyr.}$ H^4), 5.62 (br s, 2H, C$H_{pyr.}$ H^3 + H^5, $\Delta\nu_{1/2} \approx$ 120 Hz), 3.00 (br s, 2H, 2 x CHP, $\Delta\nu_{1/2} \approx$ 350 Hz), 1.26 (d, $^3J_{PH}$ = 13.6 Hz, 18H, C(CH_3)$_3$), 1.19 (br d, $^3J_{PH}$ = 13.7 Hz, 18H, C(CH_3)$_3$). ^{31}P{^{1}H} NMR (161.98 MHz, C$_6$D$_6$): δ 56.0 (s), 55.2 (s) at 298 K; δ 56.5 (s) at 343 K.

^{31}P{^{1}H} NMR (242.94 MHz, pentane with THF-d_8 insert): δ 54.8 (s), 52.9 (s) at **298 K**; δ 53.5 (d, $^2J_{P-Zr-P}$ = 5.6 Hz), 51.0 (d, $^2J_{P-Zr-P}$ = 5.6 Hz) at **233 K**.

^{13}C{^{1}H} NMR (125.77 MHz, C$_6$D$_6$, **298 K**): δ 167.5 (br d, $^2J_{PC}$ = 19.0 Hz, C$_{pyr.}$ C^2/C^6), 151.8 (br s, C$_{pyr.}$ C^6/C^2), 135.9 (s, C$H_{pyr.}$ C^4), 114.2 (br d, $^3J_{PC}$ = 12.6 Hz, C$H_{pyr.}$ C^3/C^5), 98.2 (br s, C$H_{pyr.}$ C^5/C^3), 67.4 (br d, $^1J_{PC}$ =

48.5 Hz, *C*HP), 38.7 (br d, $^1J_{PC}$ = 17.5 Hz, *C*(CH$_3$)$_3$), 38.3 (br d, $^1J_{PC}$ = 16.0 Hz, *C*(CH$_3$)$_3$), 35.5 (br d, $^1J_{PC}$ = *ca.* 13 Hz, *C*(CH$_3$)$_3$), 35.4 (br d, $^1J_{PC}$ = 22.5 Hz, *C*HP), 33.8 (br d, $^1J_{PC}$ = 13.0 Hz, *C*(CH$_3$)$_3$), 30.3 (br s, C(*C*H$_3$)$_3$), 29.5 (br s, C(*C*H$_3$)$_3$), 28.7 (br s, C(*C*H$_3$)$_3$) (assignment confirmed by ^{13}C DEPT and ^{1}H-^{13}C HSQC).

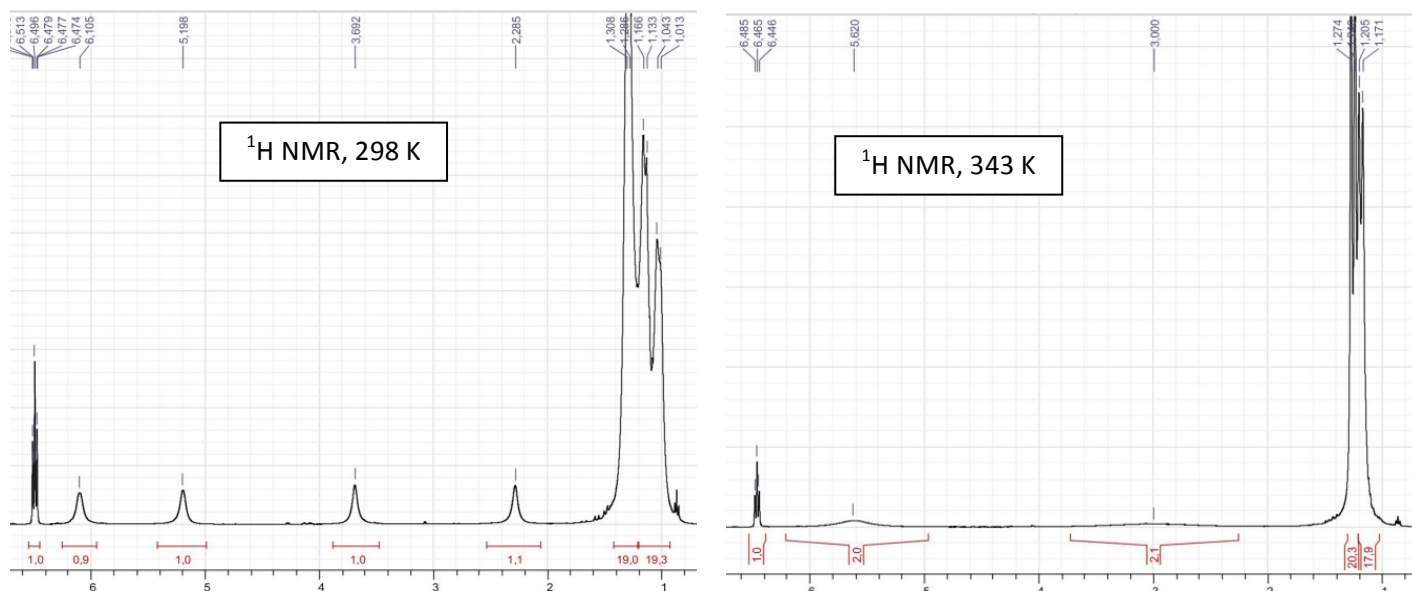### I.6.2.   Details of the ^{1}H VT NMR

Figure S2. Details of the ^{1}H NMR spectrum of [Zr(^{tBu}P*N$_a$^{tBu}P*)Cl$_2$] in C$_6$D$_6$ at different temperatures.

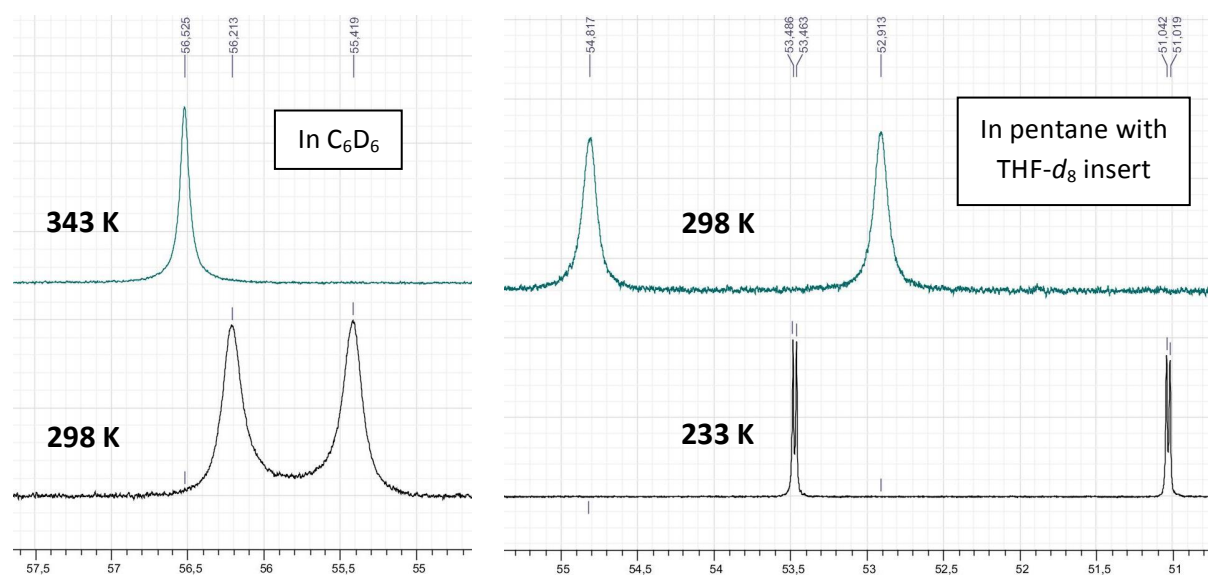### I.6.3.   Details of the ^{31}P{^{1}H} VT NMR

Figure S3. Details of the ^{31}P{^{1}H}-NMR spectrum of [Zr(^{tBu}P*N$_a$^{tBu}P*)Cl$_2$] in C$_6$D$_6$ recorded at 162 MHz (left) and in pentane along with a THF-d_8 insert recorded at 243 MHz (right) at different temperatures.

I.6.4.   Estimation of the activation energy based on $^{31}P\{^1H\}$-NMR

Crude estimation of the rate constant and the free Gibbs activation energy carried out using the approximation for a coupled AB system:[8] $k_{coal.} = \frac{\pi}{\sqrt{2}} \sqrt{(\nu_A - \nu_B)^2 + 6J_{AB}{}^2}$

Using the Eyring equation, an estimation of the energy barrier (in J·mol^{-1}) for the dynamic process can be extracted: $\Delta G^{\ddagger} = RT_c \left[23.76 - \ln(k_{coal.}/T_c)\right]$

where T_c is the coalescence temperature (in Kelvin), $\nu_{A/B}$ the chemical shifts of A/B (in Hz), J_{AB} the coupling constant between A and B (in Hz) and R the universal gas constant (8.314 J·mol^{-1}·K^{-1}).

Based on the $^{31}P\{^1H\}$-NMR:

$k_{coal.}$ = (1.32 ± 0.01) x 10^3 s^{-1} $\qquad$ $T_{coal.}$ = 320 ± 10 K $\qquad$ $\underline{\Delta G^{\ddagger} = 62 \pm 2 \text{ kJ·mol}^{-1}}$

Based on the ^1H-NMR:

$k_{coal.}$ = (1.2 ± 0.1) x 10^3 s^{-1} $\qquad$ $T_{coal.}$ = 343 ± 5 K $\qquad$ $\underline{\Delta G^{\ddagger} = 63 \pm 1 \text{ kJ·mol}^{-1}}$

These values are in agreement with the energy for the transition state of the model compound bearing Me substituents [Zr(^{Me}P*N$_a$^{Me}P*)Cl$_2$] estimated by DFT at *ca.* 63 kJ·mol^{-1}.

II.   X-RAY CRYSTALLOGRAPHY

II.1.   General methods

Suitable crystals for the X-ray analysis of all compounds were obtained as described above. Summary of the crystal data, data collection and refinement for compounds are given in Table S1. The crystals were mounted on a glass fibre with grease, from Fomblin vacuum oil. Data sets were collected at 173(2) K on a Bruker APEX-II CCD Duo diffractometer (graphite-monochromated Mo-Kα radiation, λ = 0.71073 Å). Specific comments for each data set are given below.

The cell parameters were determined (APEX2 software)[9] from reflections taken from three sets of 12 frames, each at 10 s exposure. The structures were solved by direct methods using the program SHELXS-2013.[10] The refinement and all further calculations were carried out using SHELXL-2013.[10b] The H-atoms were introduced into the geometrically calculated positions (SHELXL-2013 procedures) and refined riding on the corresponding parent atoms. The non-H atoms were refined anisotropically, using weighted full-matrix least-squares on F^2.

The following special comments apply to the models of the structures:

- The asymmetric unit of [Li$_2$(^{tBu}P*N$_a$^{tBu}P*)]$_2$ contains one half of the dimer.
- For [Cr{Cr(^{tBu}P*N$_a$^{tBu}P*)Cl}$_2$], two ^{t}Bu groups on the ligand are disordered: C41, C45 and C46 carbons atoms are disordered over two positions with an occupancy ratio of 70/30. A

squeeze procedure was applied and the residual electron density was assigned to one disordered molecule of pentane. The absolute configuration of the C6 and C29 carbon atoms is S. The space group $P2_12_12_1$ is chiral and only this configuration is present in the cell. The Flack parameter[11] is 0.002(18).

- The asymmetric unit of [Zr(^{tBu}P*N$_a$^{tBu}P*)Cl$_2$] contains two crystallographically independent molecules. Thermal motions affect some methyl groups on the ligands.

II.2. Summary of the crystal data

Table S1. Crystal data, data collection and refinement for the different compounds.

Compounds	[Li$_2$(^{tBu}P*N$_a$^{tBu}P*)]$_2$ (**1**)	[Cr{Cr(^{tBu}P*N$_a$^{tBu}P*)Cl}$_2$] (**2**)	[Zr(^{tBu}P*N$_a$^{tBu}P*)Cl$_2$] (**3**)
Chemical formula	C$_{46}$H$_{82}$Li$_4$N$_2$P$_4$	C$_{46}$H$_{82}$Cl$_2$Cr$_3$N$_2$P$_4$	C$_{23}$H$_{41}$Cl$_2$NP$_2$Zr
CCDC Number	1427661	1427662	1427663
Formula Mass	814.77	1013.91	555.63
Crystal system	Monoclinic	Orthorhombic	Orthorhombic
a/Å	16.4117(13)	17.0266(14)	15.8964(13)
b/Å	8.6059(6)	18.1629(15)	21.1004(17)
c/Å	22.4415(14)	19.1642(15)	33.285(3)
α/°	90	90	90
β/°	125.229(4)	90	90
γ/°	90	90	90
Unit cell volume/Å^3	2589.1(3)	5926.6(8)	11164.5(16)
Temperature/K	173(2)	173(2)	173(2)
Space group	$P2_1/c$	$P2_12_12_1$	$Pbca$
No. of formula units per unit cell, Z	2	4	16
Absorption coefficient, μ/mm	0.175	0.766	0.710
No. of reflections measured	18475	39878	94787
No. of independent reflections	6245	14278	13508
R_{int}	0.0435	0.1268	0.1179
Final R_1 values ($I > 2\,\sigma(I)$)	0.0582	0.0731	0.0870
Final $wR(F^2)$ values ($I > 2\,\sigma(I)$)	0.1423	0.1210	0.1267
Final R_1 values (all data)	0.0913	0.1515	0.1509
Final $wR(F^2)$ values (all data)	0.1618	0.1396	0.1408
Goodness of fit on F^2	1.018	0.898	1.195

II.3.1. <u>The crystal structure of [Li$_2$(^{tBu}P*N$_a$^{tBu}P*)]$_2$</u>
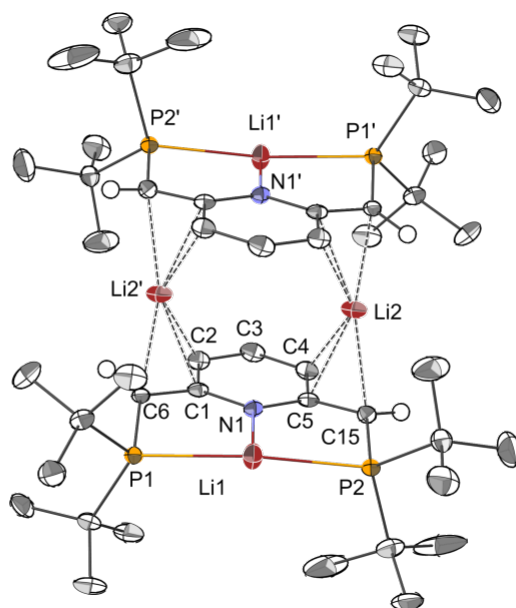
Figure S4. The structure of centrosymmetric [Li$_2$(^{tBu}P*N$_a$^{tBu}P*)]$_2$ with thermal ellipsoids at the 40% probability level. Hydrogen atoms have been omitted except for the α-CHP protons. Selected bond distances (Å) and angles [°]: Li1-N1 1.936(4), Li1-P1 2.484(4), Li1-P2 2.481(4), Li2-C4 2.480(6), Li2-C5 2.241(5), Li2-C15 2.258(5), Li2'-C1 2.284(5), Li2'-C2 2.481(6), Li2'-C6 2.212(5), P1-C6 1.783(2), P2-C15 1.778(2), C1-C6 1.426(3), C5-C15 1.425(3), C1-N1 1.374(3), C1-C2 1.425(3), C2-C3 1.382(4), C3-C4 1.380(4), C4-C5 1.425(3), C5-N1 1.374(3); P1-Li1-P2 167.6(2), C1-Li2-C5' 133.4(2), C2-Li2-C4' 137.9(2), C6-Li2-C15' 163.0(3), P1-C6-C1 118.8(2), P2-C15-C5 120.2(2).

II.3.2. <u>The crystal structure of [Zr(^{tBu}P*N$_a$^{tBu}P*)Cl$_2$]</u>
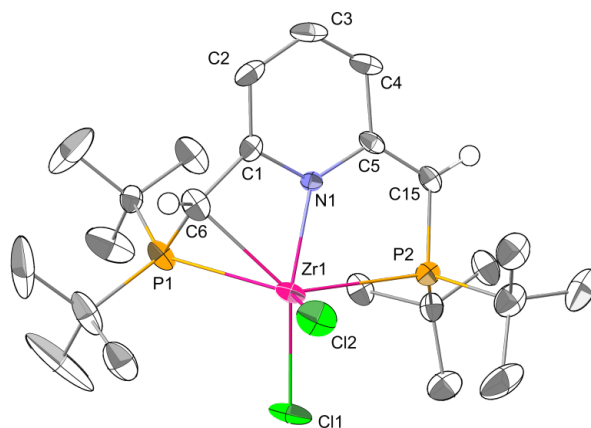
Figure S5. The molecular structure of one of the two crystallographically independent molecules of [Zr(^{tBu}P*N$_a$^{tBu}P*)Cl$_2$] with thermal ellipsoids at the 30% probability level. Selected bond distances (Å) and angles [°]: Zr1-N1 2.120(4), Zr1-C6 2.382(7), Zr1-P1 2.643(2), Zr1-P2 2.811(2), Zr1-Cl1 2.429(2), Zr1-Cl2 2.382(2), P1-C6 1.776(6), P2-C15 1.757(6), C1-C6 1.460(8), C5-C15 1.358(9), C1-C2 1.367(8), C2-C3 1.409(10), C3-C4 1.332(10), C4-C5 1.445(8), N1-C1 1.385(7), C5-N1 1.386(7); Zr1-N1-C1 99.6(4), Zr1-N1-C5 135.1(4), C1-C6-P1 117.3(5), C5-C15-P2 116.1(5), N1-C1-C6 109.8(5), N1-C5-C15 118.9(5).
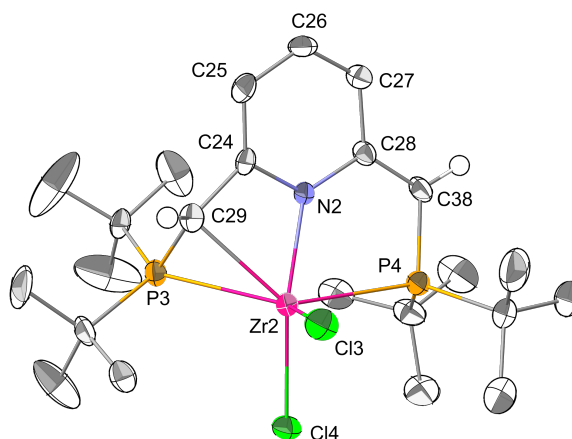
Figure S6. The molecular structure of the second crystallographically independent molecules [Zr(^{tBu}P*N$_a$^{tBu}P*)Cl$_2$] with thermal ellipsoids at the 30% probability level. Selected bond distances (Å) and angles [°]: Zr2-N2 2.134(4), Zr2-C29 2.411(6), Zr2-P3 2.622(2), Zr2-P4 2.799(2), Zr2-Cl3 2.377(2), Zr2-Cl4 2.433(2), P3-C29 1.782(6), P4-C38 1.770(6), C24-C29 1.465(7), C28-C38 1.346(8), C24-C25 1.362(8), C25-C26 1.412(8), C26-C27 1.346(8), C27-C28 1.438(7), N2-C24 1.387(7), N2-C28 1.411(6); Zr2-N2-C24 99.8(3), Zr2-N2-C38 134.0(4), C24-C29-P3 119.8(4), C28-C38-P4 117.0(4), N2-C24-C29 110.0(5), N2-C28-C38 118.1(5).

II.3.3. The crystal structure of [Cr{Cr(^{tBu}P*N$_a$^{tBu}P*)Cl}$_2$]
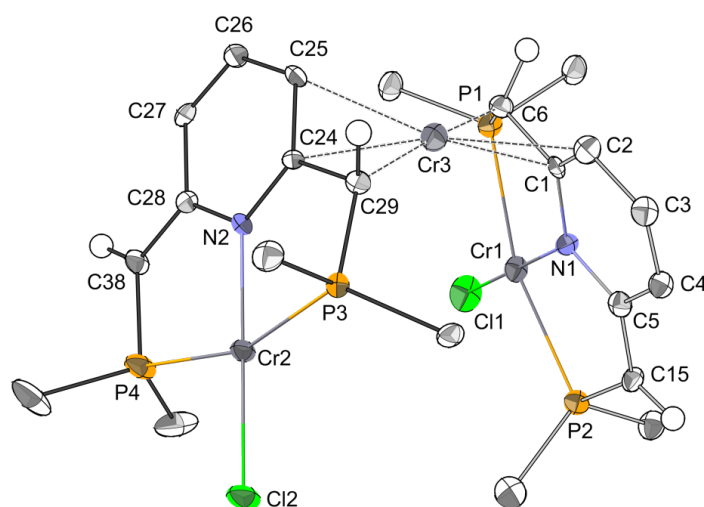
Figure S7. The structure of [Cr{Cr(^{tBu}P*N$_a$^{tBu}P*)Cl}$_2$] with thermal ellipsoids represented at the 30% probability level. For clarity, hydrogen atoms have been omitted and only one ^{t}Bu carbon is represented. Selected bond distances (Å) and angles [°]: Cr1-Cl1 2.304(2), Cr1-P1 2.439(3), Cr1-P2 2.445(3), Cr1-N1 2.052(6), Cr2-Cl2 2.325(2), Cr2-P3 2.464(2), Cr2-P4 2.470(2), Cr2-N2 2.058(6), Cr3-C1 2.334(7), Cr3-C2 2.393(8), Cr3-C6 2.175(8), Cr3-C24 2.340(7), Cr3-C25 2.362(7), Cr3-C29 2.208(8), P1-C6 1.820(8), C1-C6 1.449(10), P3-C29 1.786(8), C29-C24 1.442(10), P2-C15 1.761(7), C15-C5 1.374(10), P4-C38 1.725(8), C28-C38 1.389(10), C1-N1 1.394(9), C1-C2 1.389(10), C2-C3 1.430(11), C3-C4 1.331(10), C4-C5 1.441(10), C5-N1 1.408(9), C24-N2 1.390(9), C24-C25 1.408(10), C25-C26 1.416(10), C26-C27 1.320(10), C27-C28 1.446(10), C28-N2 1.408(9); P2-Cr1-P1 161.60(9), P1-Cr1-Cl1 98.94(9), Cl1-Cr1-P2 97.61(9), N1-Cr1-P1 80.7(2), P2-Cr1-N1 82.6(2), P3-Cr2-N2 81.2(2), P4-Cr2-Cl2 98.09(9), N2-Cr2-P4 82.2(2), Cl2-Cr2-P3 98.44(8), P2-C15-C5 119.9(6), C1-C6-P1 112.0(5), C24-C29-P3 115.1(6), C28-C38-P4 120.7(6). Sum of the angles around Cr1 ≈ 359.9°; around Cr2 ≈ 359.9°.

III.   COMPUTATIONAL METHODS

Geometry optimisations without constraint of all compounds were carried out with the Gaussian 09 program[12] at the M06-2X level.[13] All calculations at the M06-2X DFT level were conducted with the "Ultrafine" grid option for integration, as implemented in the Gaussian 09 package. Hydrogen, carbon, nitrogen, phosphorus and chlorine atoms were described with the 6-31++G(d,p) basis set.[14] The Stuttgart-Dresden-Bonn (SDB) energy-consistent quasi-relativistic effective core potential (ECP28MWB) and its associated valence basis set were employed to model the Zr atom.[15] To get accurate geometries, the SCF convergence criterion was systematically tightened to 10^{-8} au and the force minimisations were carried out until the rms force became smaller than (at least) 1×10^{-5} au ("tight" optimisation in Gaussian 09). Selected bond lengths of $^{Me}PN^{Me}P$, $^{Me}PN_a{}^{Me}P*$ and $^{Me}P*N_a{}^{Me}P*$ in their optimised geometry are given in Figure S8.
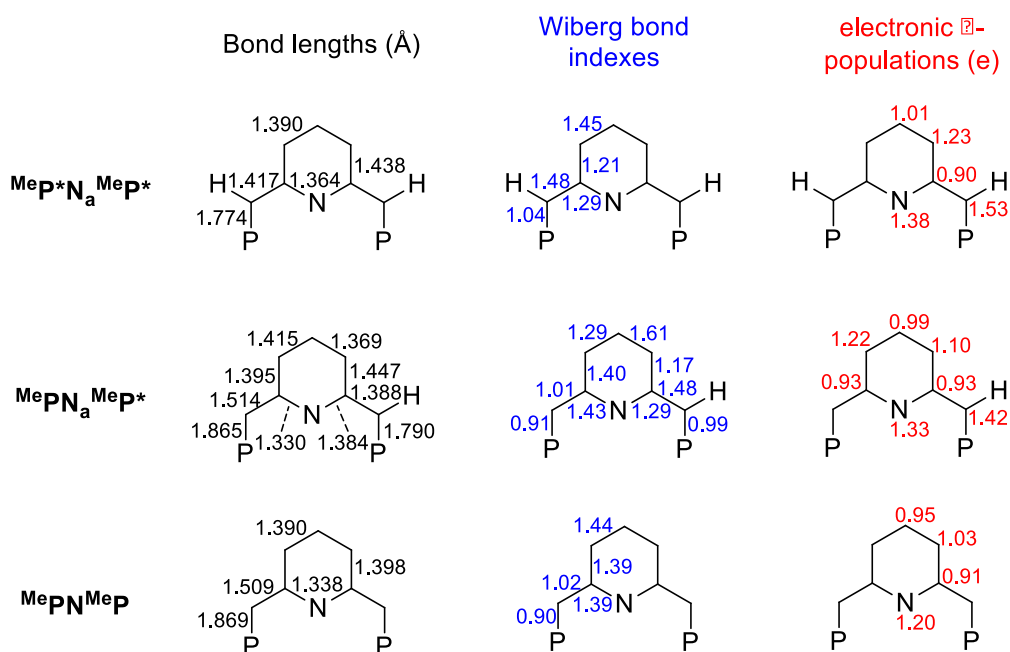
Figure S8. Bond lengths, Wiberg bond indexes and electronic π-populations calculated for $^{Me}P*N_a{}^{Me}P*$, $^{Me}PN_a{}^{Me}P*$ and $^{Me}PN^{Me}P$ at the M06-2X/6-31++G(d,p) level of theory.

The nature of each stationary point was confirmed by harmonic frequency calculations at the same level, and all geometries were found to represent minima on the potential energy surface, with the exception of the Zr complex **TS3'-3'** which was found to be the symmetric transition state for the oscillation of the Zr centre within the ligand pocket from **3'** (Figure S9).
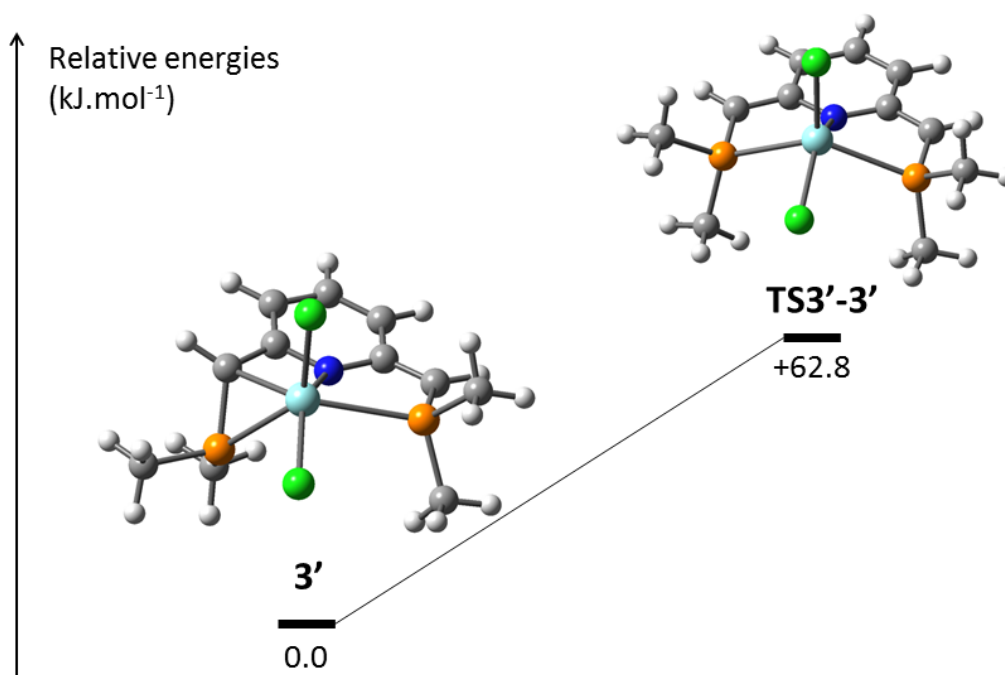
Figure S9. Potential energy surface for oscillation of the metal centre within the ligand pocket from [Zr(^{Me}P*N$_a$^{Me}P*)Cl$_2$] (**3′**). Calculations at the M06-2X level with the 6-31++G(d,p) basis set for H, C, N, P and Cl atoms and the SDB effective core potential (ECP28MWB) and its associated valence basis set for Zr.

Nucleus-independent chemical shifts (NICS)[16] were calculated for ^{Me}PN^{Me}P, ^{Me}PN$_a$^{Me}P* and ^{Me}P*N$_a$^{Me}P* by using the gauge invariant atomic orbital (GIAO) method[17] at the M06-2X/6-31++G(d,p) level at the pyridine ring centre. The same level of calculation has been used to obtain molecular orbitals (MOs) of ^{Me}PN^{Me}P, ^{Me}PN$_a$^{Me}P* and ^{Me}P*N$_a$^{Me}P* depicted in Figures S10, S11 and S12, respectively. The occupied and delocalised π-molecular orbitals are the HOMO-2, HOMO-4 and HOMO-10 for ^{Me}PN^{Me}P, the HOMO, HOMO-4, HOMO-5 and HOMO-11 for ^{Me}PN$_a$^{Me}P*, and the HOMO, HOMO-1, HOMO-4, HOMO-5 and HOMO-12 for ^{Me}P*N$_a$^{Me}P*. It should be noted that the HOMO of ^{Me}P*N$_a$^{Me}P* is the out-of-phase combination of two non-bonding type MOs of allyl groups (the two CH$_{α-P}$, C$_{α-N}$ and C$_{β-N}$ moieties), which is fully consistent with η^3-allylic-type interactions observed for [Li$_2$(^{tBu}P*N$_a$^{tBu}P*)]$_2$ and [Cr{Cr(^{tBu}P*N$_a$^{tBu}P*)Cl]$_2$]. The nitrogen and phosphorus σ lone pairs (localised MOs or delocalised in-phase and out-of-phase combinations) correspond to the HOMO, HOMO-1 and HOMO-3 for ^{Me}PN^{Me}P, the HOMO-1, HOMO-2 and HOMO-3 for ^{Me}PN$_a$^{Me}P*, and the HOMO-2, HOMO-3 and HOMO-4 for ^{Me}P*N$_a$^{Me}P*. The remaining MOs in Figure S10-S12 correspond to σ-bonds of the molecular backbones.

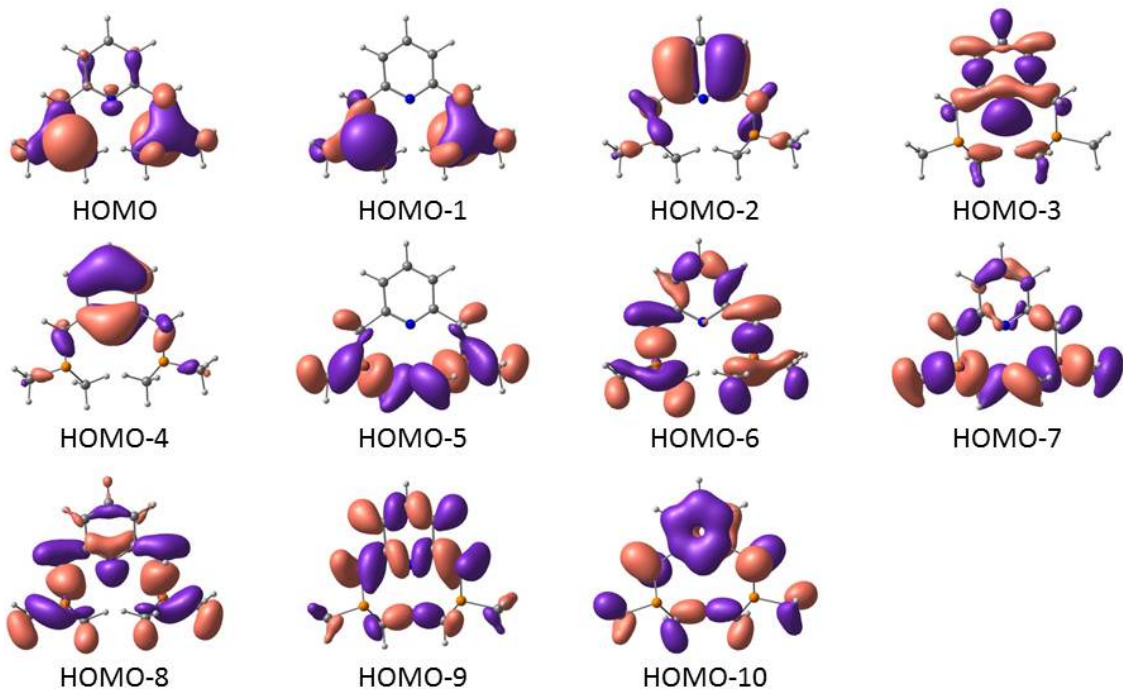HOMO   HOMO-1   HOMO-2   HOMO-3

HOMO-4   HOMO-5   HOMO-6   HOMO-7

HOMO-8   HOMO-9   HOMO-10

Figure S10. Highest occupied molecular orbitals of $^{Me}PN^{Me}P$ (isosurface contour value= 0.03 au).

HOMO   HOMO-1   HOMO-2   HOMO-3

HOMO-4   HOMO-5   HOMO-6   HOMO-7

HOMO-8   HOMO-9   HOMO-10   HOMO-11
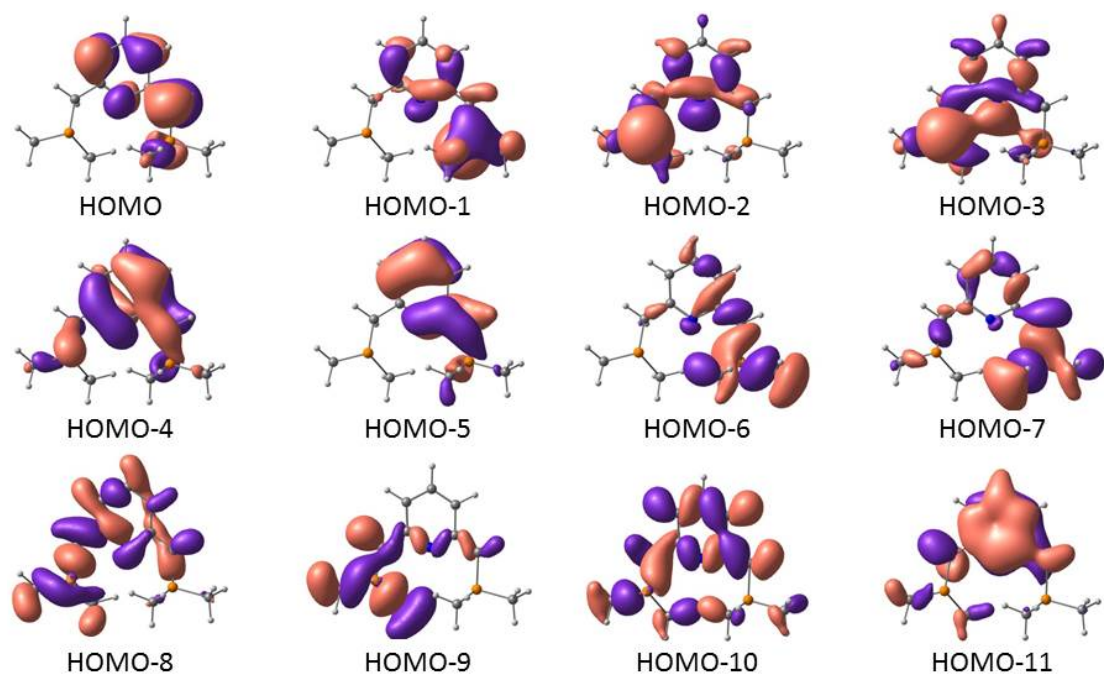
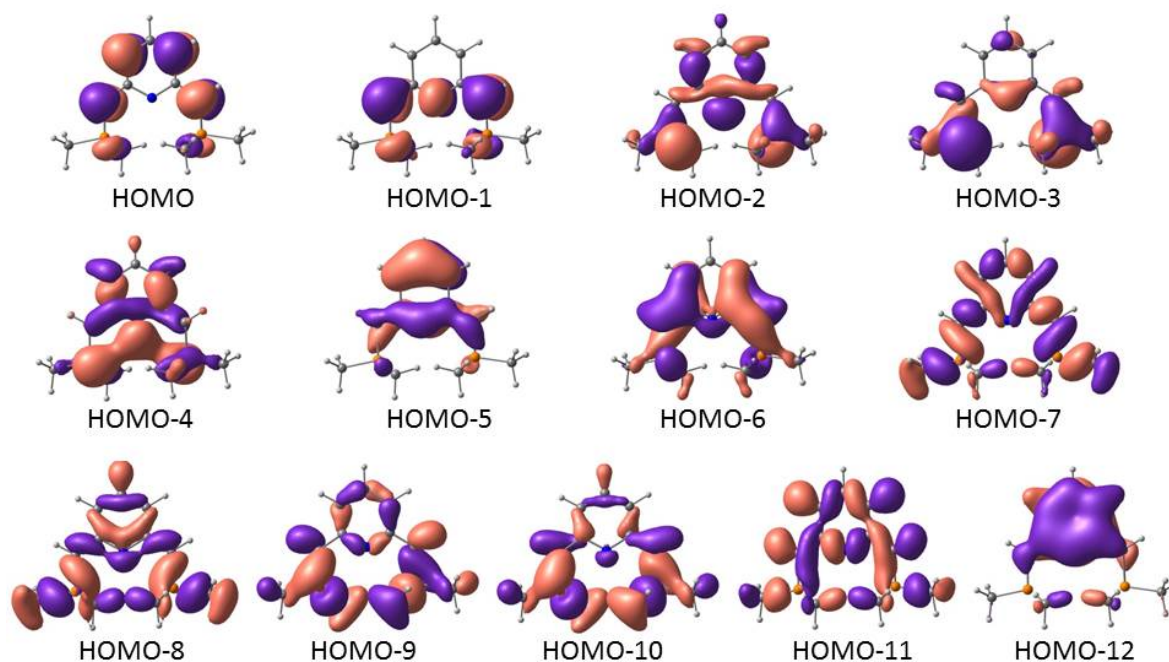**Figure S11.** Highest occupied molecular orbitals of $^{Me}PN_a^{Me}P^*$ (isosurface contour value= 0.03 au).

Figure S12. Highest occupied molecular orbitals of $^{Me}P^*N_a{}^{Me}P^*$ (isosurface contour value= 0.03 au).

Electronic structures obtained at the M06-2X/6-31++G(d,p) level for $^{Me}PN^{Me}P$, $^{Me}PN_a{}^{Me}P^*$ and $^{Me}P^*N_a{}^{Me}P^*$ were explored by means of natural bond orbital (NBO) analysis[18] using the NBO6 program.[19] The NBO procedure has been use to obtain the Wiberg bond index, as well as the π-electron population computed from the occupancy of the p_x natural atomic orbitals (similar values are obtained from the occupancy and polarisation of the natural π-bond orbitals) (Figure S8). It was also used to evaluate the relative contribution of the resonance structures of $^{Me}PN^{Me}P$, $^{Me}PN_a{}^{Me}P^*$ and $^{Me}P^*N_a{}^{Me}P^*$ by means of natural resonance theory (NRT).[20] These calculations have used the multi-reference NRT analysis. Reference resonance structures correspond to the structures, which do not show charge separation (Figures S13-S15). Single-reference NRT calculations give almost similar weights. The NRT analysis has been confined to the C_5N pyridine ring, the C_5N-$C_{\alpha-P}$ and the $C_{\alpha-P}$-C_5N-$C_{\alpha-P}$ atoms for $^{Me}PN^{Me}P$, $^{Me}PN_a{}^{Me}P^*$ and $^{Me}P^*N_a{}^{Me}P^*$, respectively. Despite this restriction, a very large number of structures with significant weight is obtained, as shown in Figures S13-S15. In order to simplify the analysis, only resonance structures with a weight larger than 5% have been considered, and the weights have been rescaled to amount to a total of 100%. For $^{Me}PN^{Me}P$, this leads to two resonance structures (a and b, Figure S13) with a weight of 50%. Similar analysis leads to the data indicated in Figure S16 and Scheme 1 for $^{Me}PN_a{}^{Me}P^*$ and $^{Me}P^*N_a{}^{Me}P^*$, respectively.

Figure S13. NRT resonance structures calculated for $^{Me}PN^{Me}P$ through a multi-reference NRT analysis based on resonance structures a and b. A total of 36 resonance structures have been obtained. Only resonance structures with a weight larger than 1% are depicted.
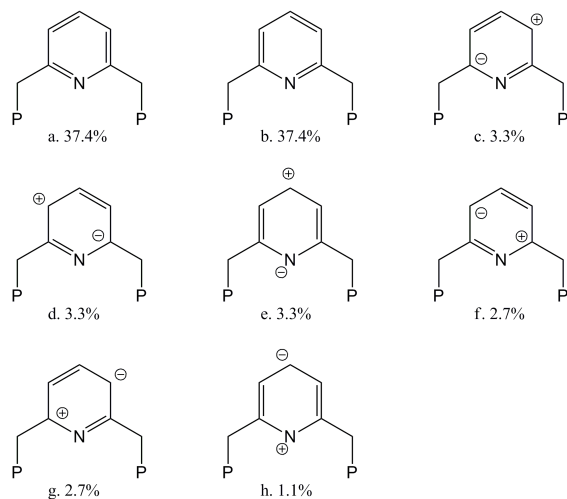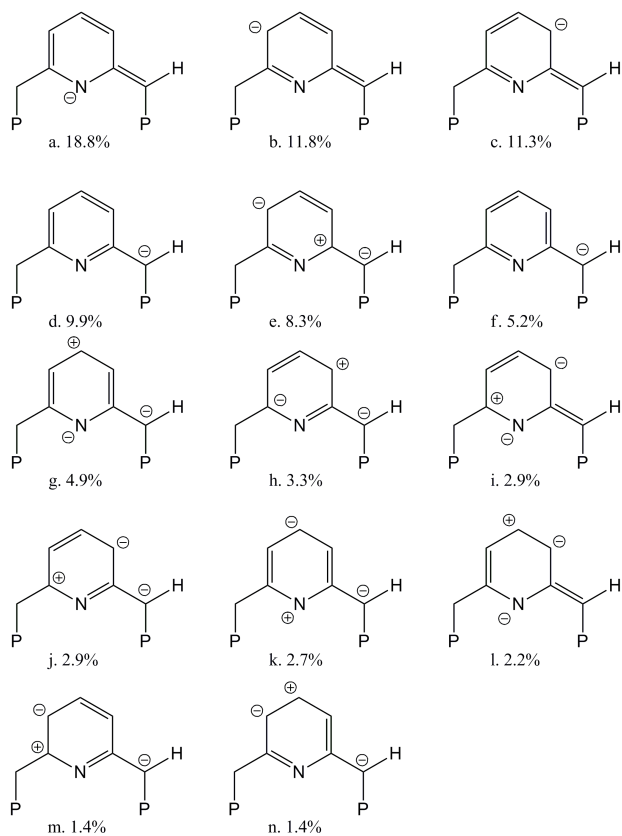

Figure S14. NRT resonance structures calculated for $^{Me}PN_a{}^{Me}P^*$ through a multi-reference NRT analysis based on resonance structures a, b, c, d and f. A total of 106 resonance structures have been obtained. Only resonance structures with a weight larger than 1% are depicted.
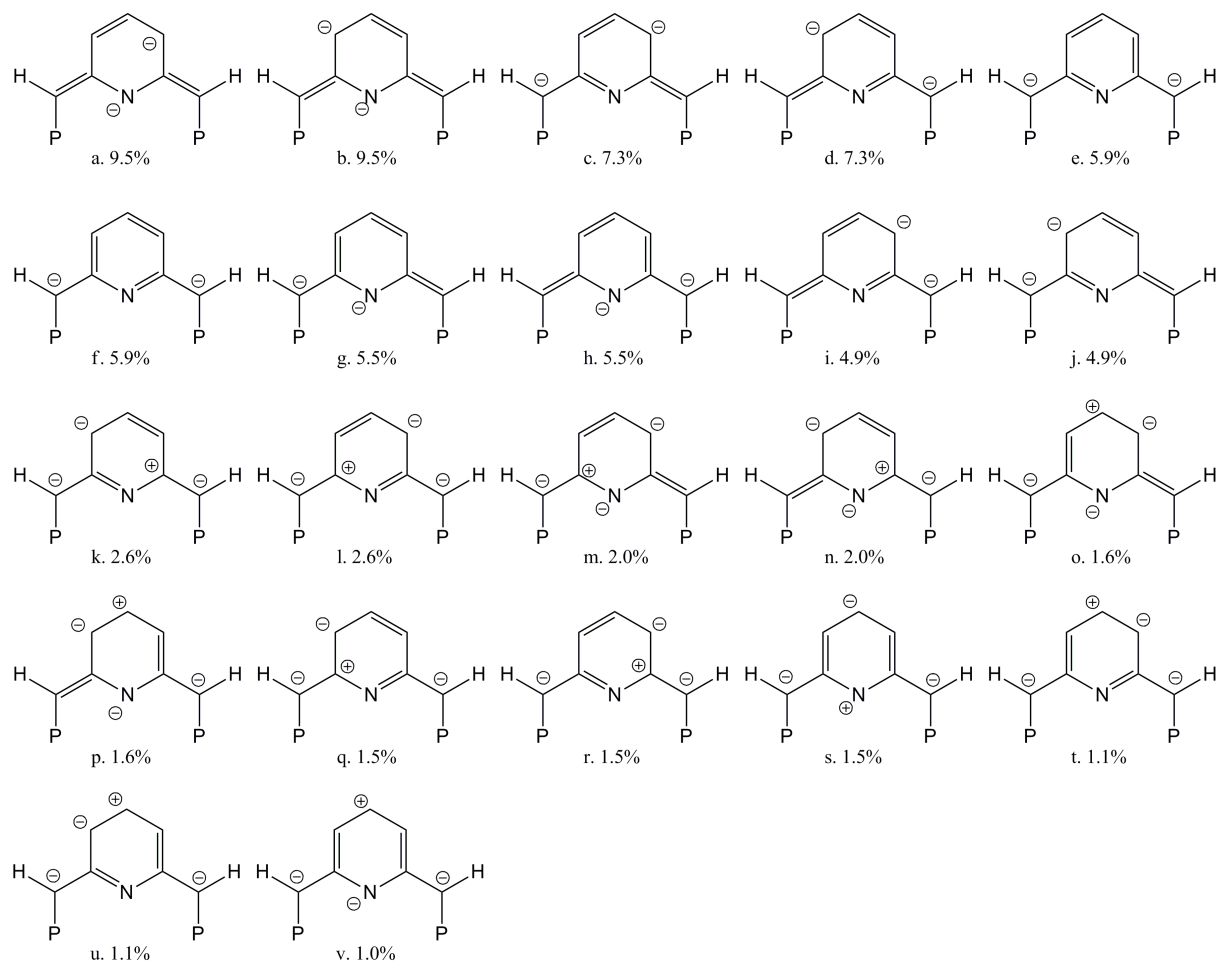
Figure S15. NRT resonance structures calculated for $^{Me}P*N_a{}^{Me}P*$ through a multi-reference NRT analysis based on resonance structures a-j. A total of 300 resonance structures have been obtained. Only resonance structures with a weight larger than 1% are depicted.
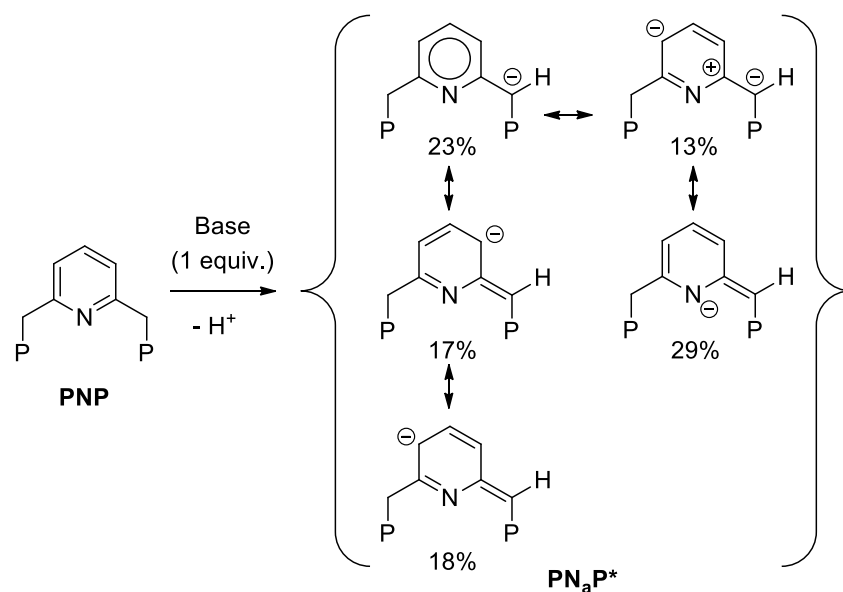

Figure S16. Deprotonation of $^RPN^RP$ and relevant resonance structures of $^RPN_a{}^RP*$. NBO weight of the resonance structures calculated for R = Me at the M06-2X/6-31++G(d,p) level of theory.

Second-order perturbation theory has been used to estimate the second-order interaction energy associated with two-electron donor-acceptor orbital interactions. The $C_{\alpha-P}$ lone pair $\rightarrow \sigma^*$ P-C_{Me} interaction (*i.e.* hyperconjugation) has been estimated for $^{Me}PN_a^{Me}P^*$ and $^{Me}P^*N_a^{Me}P^*$ based on the resonance structures d-g (for $^{Me}PN_a^{Me}P^*$, Figure S14) and c-j (for $^{Me}P^*N_a^{Me}P^*$, Figure S15). Equal values (73 kJ.mol^{-1} for $^{Me}PN_a^{Me}P^*$; 95 kJ.mol^{-1} for $^{Me}P^*N_a^{Me}P^*$ for each individual $C_{\alpha-P}$ lone pair) are obtained independently of the considered resonance structure.

An Energy Decomposition Analysis (EDA)[21] of the $^{Me}P^*N_a^{Me}P^*$ ligand – Zr transition metal bond in **3'** was done at the BP86[22] using the Extended Transition State (ETS) scheme[23] with the ADF2013.01c program,[24] based on the M06-2X geometries. Uncontracted Slater-type orbitals were used as basis functions. All elements were described by basis sets of triple-ξ quality augmented by two sets of polarisation functions (basis set called TZ2P in ADF).[25] Core electrons for Zr ("Zr.3d" basis set) were treated with the frozen-core approximation. Scalar relativistic effects were accounted for by applying the zeroth-order regular approximation (ZORA).[26] The instantaneous interaction energy ΔE_{int} between two molecular fragments A and B in the frozen geometry of molecule AB is decomposed into three main components:

$\Delta E_{int} = \Delta E_{elstat} + \Delta E_{Pauli} + \Delta E_{orb}$

The term ΔE_{elstat} corresponds to the electrostatic interaction between the unperturbed charge distributions of fragments A and B. The Pauli repulsion term ΔE_{Pauli} describes the energy change arising from the repulsive interaction caused by the Pauli exclusion principle, that is the destabilizing interaction of same spin electrons on fragments A and B. The orbital interaction term ΔE_{orb} is the energy gained by the relaxation of the molecular orbitals to their optimal form and accounts for charge transfer and polarisation effects.

The ETS-NOCV (Natural Orbitals for Chemical Valence) scheme, computed at the same level of theory, was used to investigate the orbital interaction energy ΔE_{orb}.[27] Within this framework, it is possible to separate the orbital interactions between ligand and transition metal fragment into contributions related to the deformation density due to the bonding. Each individual deformation density contribution is associated with an energy contribution to the total bond energy. Complementary NOCVs with opposite sign and identical absolute energy eigenvalues can be grouped together to describe charge transfer channels between the molecular fragments. Visualisation allows the assignment of these NOCV pairs to donating and back-donating processes and sometimes identification of the participating fragment orbitals.

Cartesian Coordinates of the optimised geometries

^{Me}PN^{Me}P
C -2.078838 0.332854 -0.159204
C -0.680977 0.329936 -0.162742
C -0.009278 1.530534 0.036537
C -0.747049 2.693459 0.225286
C -2.142550 2.615879 0.200879
N -2.784468 1.456357 0.015805
H 1.076240 1.559548 0.044646
H -0.139616 -0.598697 -0.313071
H -0.258370 3.649623 0.383310
C -2.990486 3.854624 0.356333
H -3.076352 4.362676 -0.615105
C -2.856978 -0.949355 -0.326805
H -2.930066 -1.461664 0.643441
P -4.575203 -0.703559 -1.019070
P -4.703262 3.517125 1.022988
C -5.578945 3.118891 -0.561341
H -5.195191 2.177034 -0.961885
H -6.649678 3.004964 -0.366648
H -5.438167 3.908548 -1.308370
C -5.236427 5.290546 1.183912
H -4.732277 5.759169 2.033629
H -5.024340 5.871505 0.279149
H -6.312886 5.324542 1.374375
C -5.494441 -0.353302 0.551864
H -5.167562 0.607548 0.957714
H -6.566709 -0.296654 0.341177
H -5.322842 -1.134611 1.301222
C -5.010421 -2.502863 -1.187219
H -6.080568 -2.594233 -1.393699
H -4.469344 -2.943553 -2.029136
H -4.781121 -3.072023 -0.279162
H -2.493826 4.556062 1.036308
H -2.313470 -1.622983 -0.999023

^{Me}PN_a^{Me}P*
C -2.154170 0.342682 -0.289550
C -0.731445 0.332189 -0.023233
C -0.081545 1.489841 0.309827
C -0.791960 2.710878 0.390839
C -2.157604 2.656323 0.110438
N -2.826076 1.549380 -0.201719
H 0.988343 1.469681 0.514188
H -0.196364 -0.611822 -0.090439
H -0.308640 3.643993 0.659869
C -2.992835 3.918564 0.147829
H -3.186331 4.272570 -0.875497
C -2.869611 -0.804482 -0.604458
H -2.361933 -1.766967 -0.610804
P -4.615575 -0.716574 -0.991267
P -4.631699 3.665726 1.002233

C -5.669232 3.084136 -0.417440
H -5.304349 2.104872 -0.738559
H -6.714072 2.997436 -0.100770
H -5.607392 3.779654 -1.264109
C -5.179163 5.453345 0.986991
H -4.606384 6.030413 1.719725
H -5.049526 5.911105 -0.001985
H -6.237199 5.513835 1.262104
C -5.418951 -0.545486 0.694151
H -5.102963 0.414391 1.115778
H -6.513236 -0.552825 0.609928
H -5.091073 -1.346844 1.367458
C -4.947152 -2.538743 -1.222684
H -6.025547 -2.717721 -1.285257
H -4.486639 -2.880942 -2.154681
H -4.536546 -3.125775 -0.391011
H -2.455293 4.714073 0.677958

$^{Me}P*N_a{}^{Me}P*$
C -2.217055 0.321370 -0.282077
C -0.779190 0.340663 -0.290772
C -0.130757 1.530606 0.016712
C -0.845339 2.682734 0.321591
C -2.282018 2.622275 0.307401
N -2.920177 1.453216 0.011379
H 0.962811 1.560946 0.018802
H -0.229117 -0.561994 -0.547816
H -0.347146 3.614474 0.580638
C -3.068397 3.765460 0.594723
H -2.577174 4.725214 0.754845
C -2.937737 -0.863628 -0.572279
H -2.393449 -1.794652 -0.730432
P -4.700075 -0.844448 -0.777103
P -4.827729 3.648582 0.792809
C -5.525917 3.610645 -0.955141
H -5.216474 2.657103 -1.394247
H -6.624933 3.662185 -0.943455
H -5.111618 4.436192 -1.551507
C -5.191421 5.464493 1.103914
H -4.844897 5.748459 2.103866
H -4.679140 6.094837 0.361610
H -6.270597 5.647918 1.042921
C -5.405969 -0.845453 0.968162
H -5.151551 0.123735 1.408341
H -6.500384 -0.957844 0.952278
H -4.948820 -1.646821 1.566199
C -4.961341 -2.677699 -1.089393
H -6.028914 -2.920679 -1.032510
H -4.595783 -2.941916 -2.087980
H -4.417745 -3.278747 -0.345064

3′
C 2.701813 8.107037 27.776586
C 2.285868 6.799478 27.717998

H 1.282402 6.544407 27.401479
C 3.223540 5.811751 28.137069
H 2.916660 4.769124 28.143199
C 4.494036 6.127494 28.536411
H 5.193196 5.358123 28.844173
C 4.945656 7.493634 28.494443
C 1.986708 9.369606 27.483373
H 1.110430 9.308560 26.840257
C 0.487842 11.552393 28.608456
C 1.252650 9.363723 30.368763
C 6.236558 7.940580 28.716096
H 7.028979 7.254646 28.991705
C 7.981766 9.814414 27.276627
C 7.012454 10.563988 29.869027
N 3.979588 8.428661 28.158716
P 1.865594 10.400604 28.979960
P 6.507162 9.646061 28.356342
Cl 4.545100 12.728602 27.853249
Cl 4.518189 10.223872 25.045618
Zr 4.059646 10.420913 27.356000
H 0.359634 12.254316 29.435435
H 0.733632 12.125484 27.710662
H -0.445312 11.005896 28.444119
H 1.186358 9.960287 31.281825
H 0.272573 8.943140 30.126339
H 1.961598 8.547249 30.529327
H 6.210274 10.503163 30.607862
H 7.186174 11.614711 29.621211
H 7.920896 10.124900 30.291487
H 8.174755 10.872564 27.080834
H 8.856559 9.368506 27.758918
H 7.789310 9.305353 26.330465

TS3'-3'
C 2.458576 8.098254 27.743956
C 1.915943 6.838032 27.424339
H 0.854625 6.766921 27.221095
C 2.740658 5.724146 27.383288
H 2.312529 4.755840 27.136741
C 4.095691 5.813384 27.663477
H 4.737830 4.941517 27.647117
C 4.662173 7.062394 27.985711
C 1.648570 9.249545 27.799155
H 0.594771 9.148617 27.561919
C 1.555213 12.150711 27.423203
C 1.983970 11.180255 30.091502
C 6.034058 7.188030 28.280282
H 6.654835 6.299924 28.226763
C 8.371135 8.946706 28.170968
C 6.889633 8.874219 30.629695
N 3.841861 8.206290 27.981183
P 2.325147 10.757131 28.330732
P 6.668113 8.715605 28.807192
Cl 5.541530 12.030542 28.874624

Cl 5.199154 10.479155 25.348067
Zr 4.779796 10.120483 27.633721
H 1.972341 13.097732 27.775075
H 1.748724 12.041359 26.354474
H 0.474223 12.148210 27.592705
H 2.485809 12.114966 30.357402
H 0.905202 11.278032 30.245581
H 2.360537 10.375134 30.726401
H 5.928513 8.697914 31.117838
H 7.242851 9.878794 30.879289
H 7.607816 8.127294 30.980915
H 8.771136 9.901778 28.520960
H 9.011493 8.135039 28.529320
H 8.357567 8.934696 27.079521

IV.   NMR SPECTRA

IV.1.   [Li$_2$(^{tBu}P*N$_a$^{tBu}P*)]$_2$

^{1}H NMR (400.13 MHz, C$_6$D$_6$)
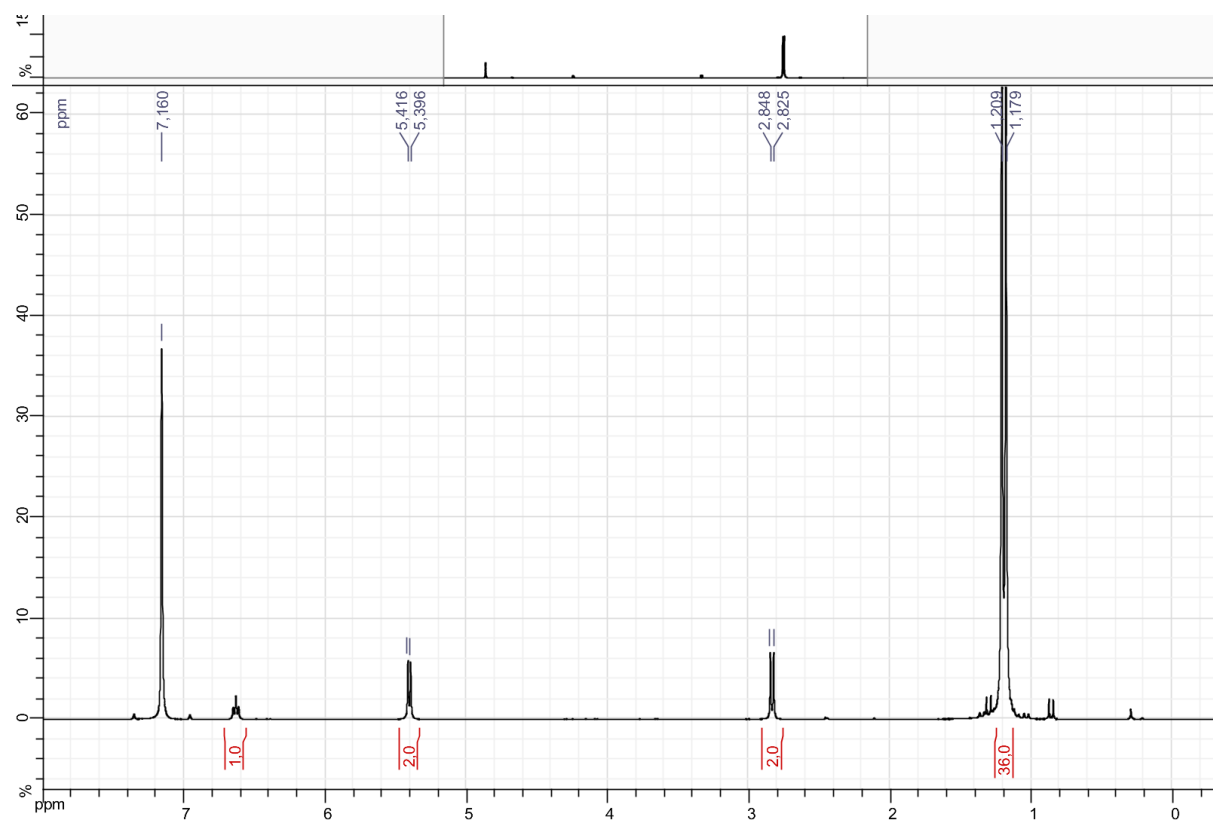
Figure S17. ^{1}H NMR spectrum of **1** in C$_6$D$_6$ (residual protio solvent from C$_6$D$_6$ at δ 7.16)

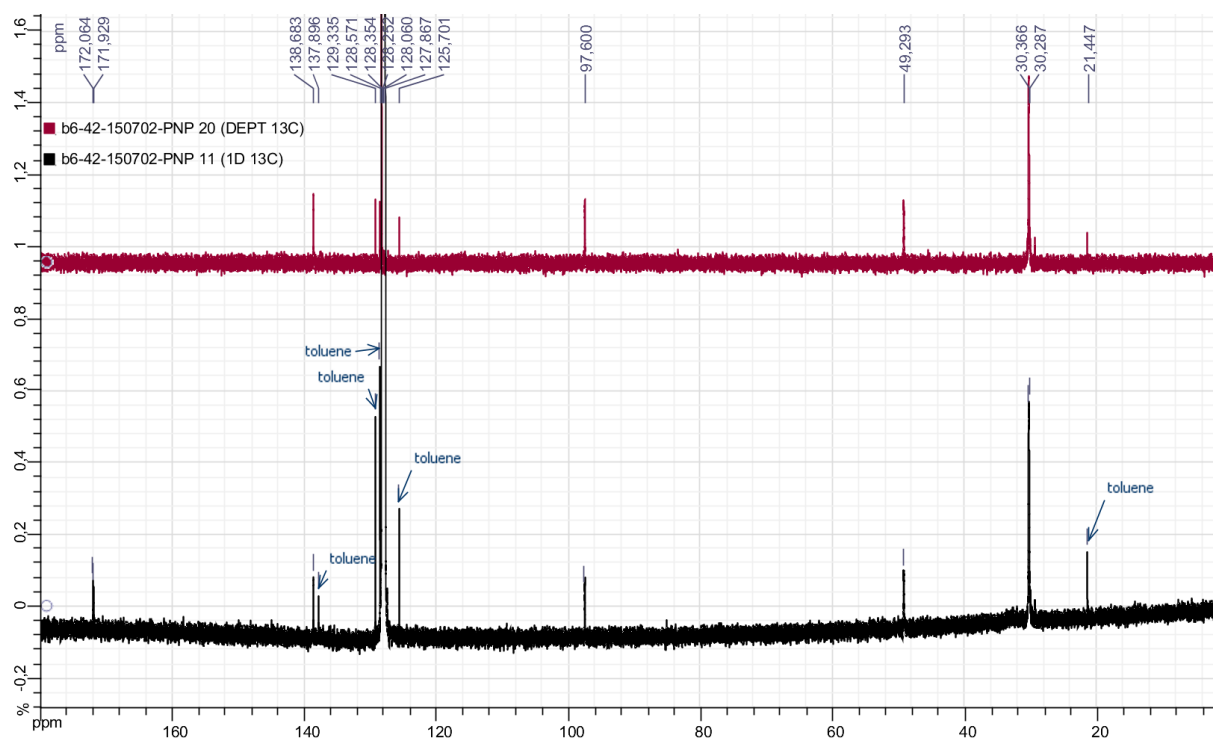## $^{13}C\{^1H\}$ NMR (125.77 MHz, C$_6$D$_6$)

Figure S18. $^{13}C\{^1H\}$ (bottom) and ^{13}C-DEPT (top) NMR spectra of **1** in C$_6$D$_6$ (solvent signals at δ 128.06). Traces of toluene are present from the sample preparation (absent in the ^1H NMR spectrum).
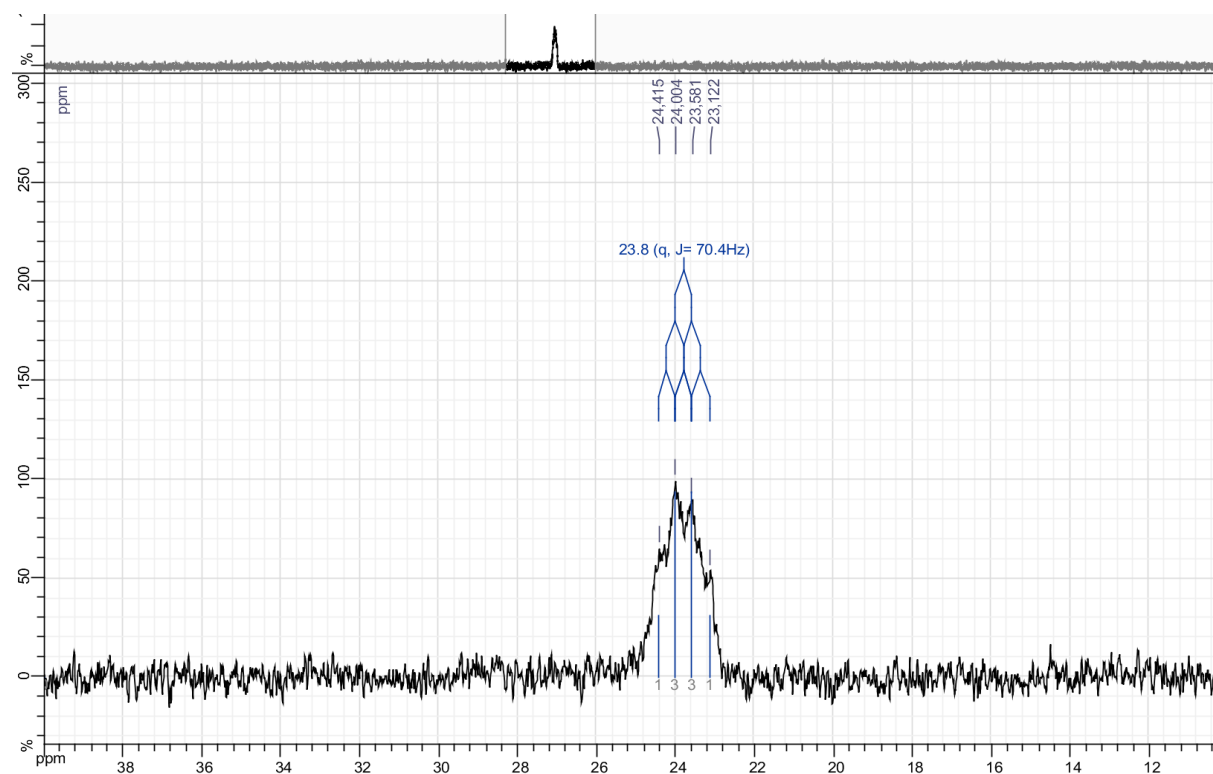
$^{31}P\{^1H\}$ NMR (161.98 MHz, C$_6$D$_6$)

Figure S19. $^{31}P\{^1H\}$ NMR spectrum of **1** in C$_6$D$_6$. The apparent quadruplet is due to the ^1J coupling with ^{7}Li (92%, I = 3/2).
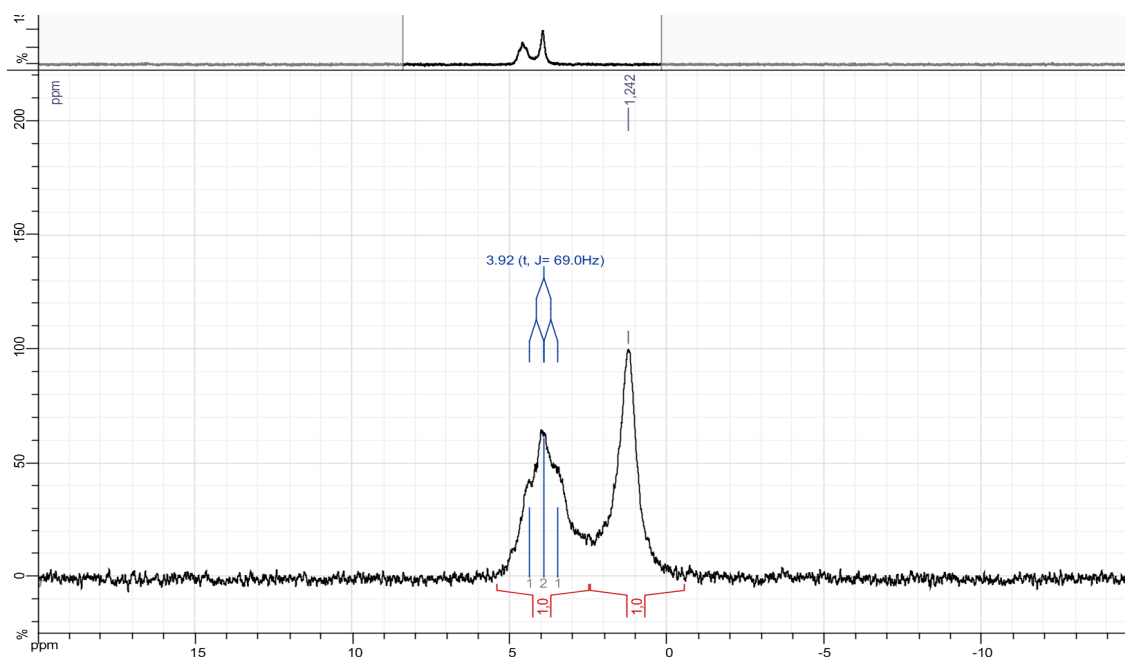
^{7}Li NMR (155.50 MHz, C$_6$D$_6$)

Figure S20. ^{7}Li NMR spectrum of **1** in C$_6$D$_6$. The apparent triplet is due to the ^1J coupling with two equivalent ^{31}P nuclei.

IV.2. K$_2$(^{tBu}P*N$_a$^{tBu}P*)

^{1}H NMR (400.13 MHz)
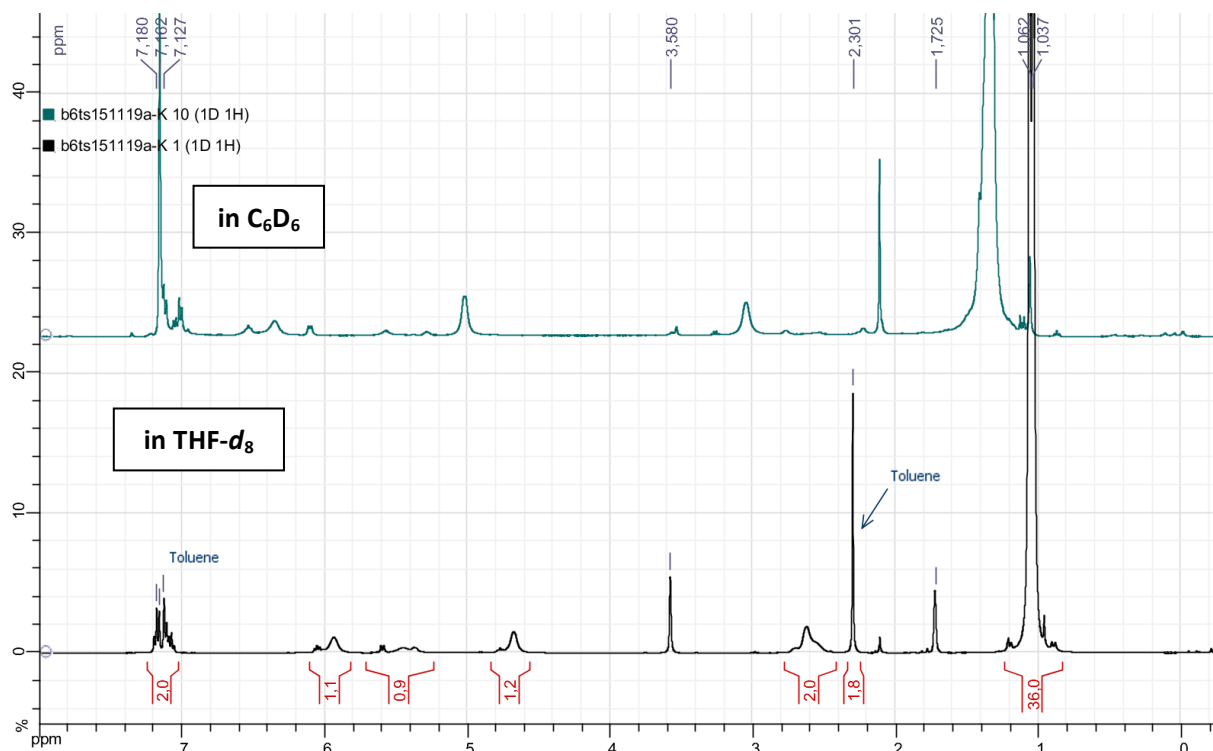
Figure S21. ^{1}H NMR spectrum of K$_2$(^{tBu}P*N$_a$^{tBu}P*) in THF-d_8 (bottom, residual protio solvent from THF-d_8 at δ 3.58 and 1.73) and after evaporation and re-dissolution in C$_6$D$_6$ (top). The compound, obtained from ^{tBu}PN^{tBu}P and KBn, is a toluene adduct formulated as K$_2$(^{tBu}P*N$_a$^{tBu}P*)·0.6 toluene.

$^{31}P\{^1H\}$ NMR (161.98 MHz)
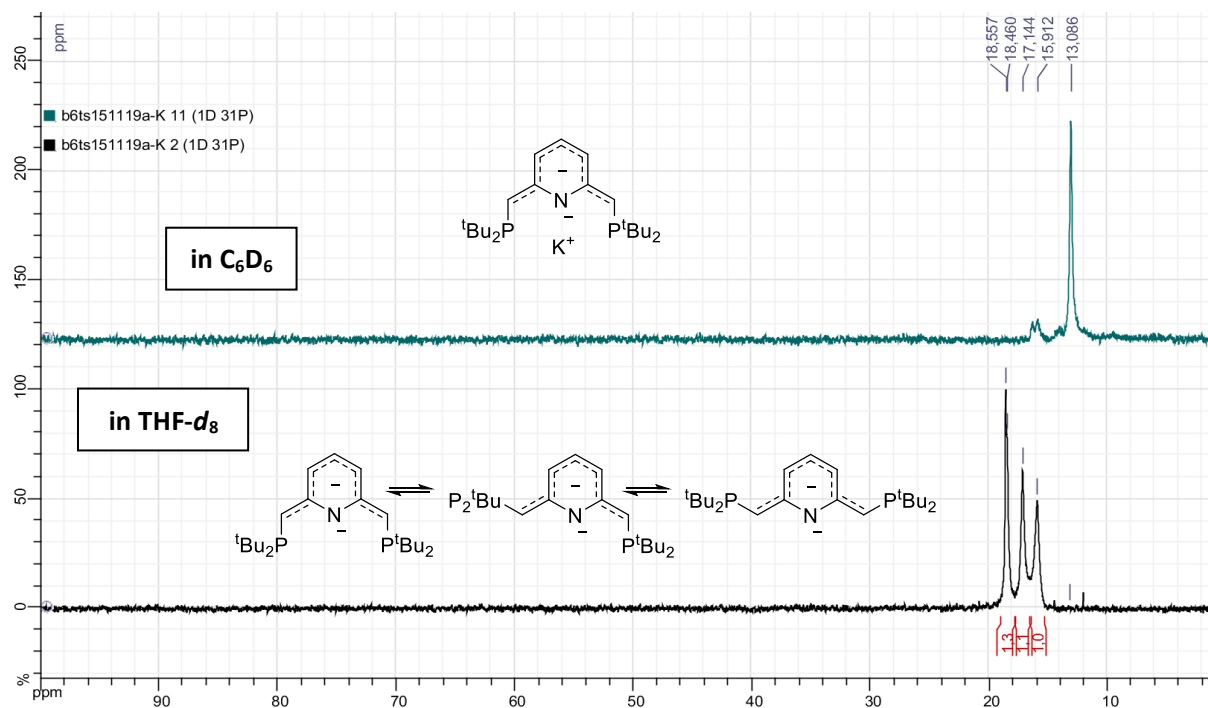
Figure S22. $^{31}P\{^1H\}$ NMR spectrum of $K_2(^{tBu}P*N_a{}^{tBu}P*)$ in THF-d_8 (bottom) and after evaporation and re-dissolution in C_6D_6 (top). Isomerisation of the exocyclic partial double bonds in THF (*vide supra*), similarly to the phenomenon described for $K(P*N_aC^{NHC})$,[4] may explain the different peaks observed.

$^{13}C\{^1H\}$ NMR (125.77 MHz, THF-d_8)
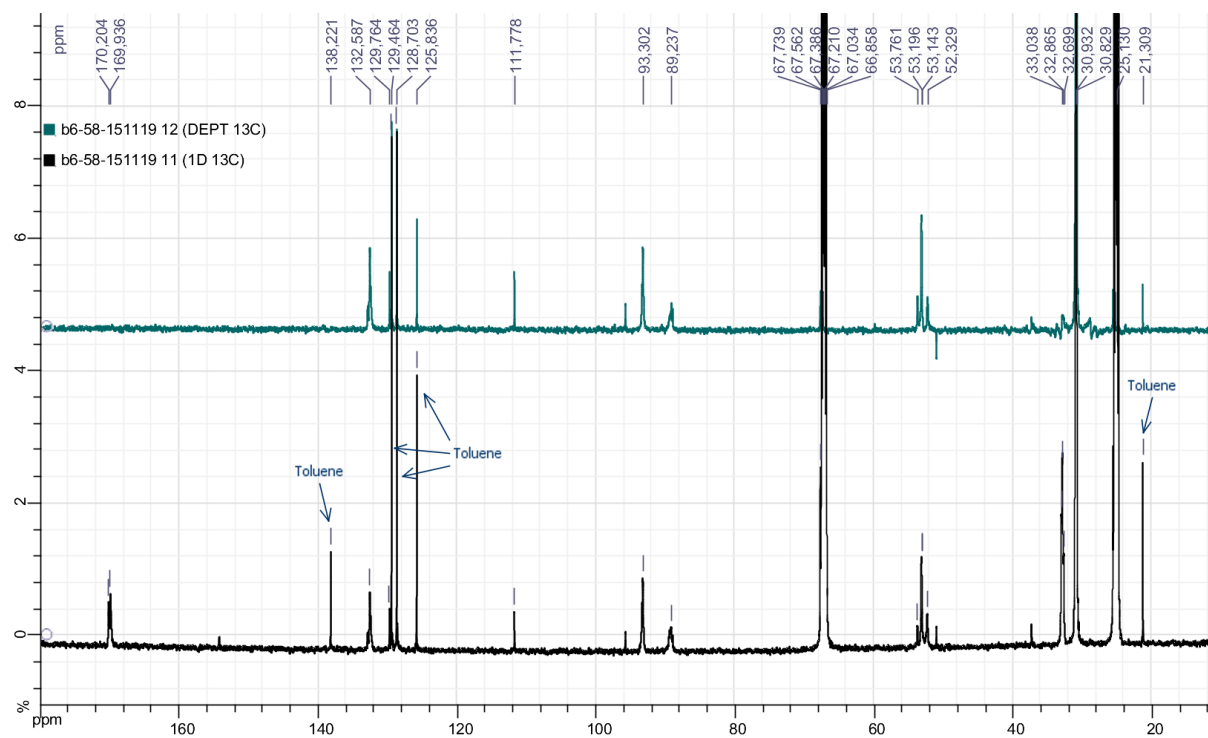
Figure S23. $^{13}C\{^1H\}$ (bottom) and ^{13}C-DEPT (top) NMR spectra of $K_2(^{tBu}P*N_a{}^{tBu}P*)$ in THF-d_8. Broad peaks are due to possible isomerisation in solution (*vide supra*). Toluene originates from the formulation $K_2(^{tBu}P*N_a{}^{tBu}P*)\cdot0.6$ toluene. An unidentified impurity is present at δ 111.8.

IV.3. α,α'-*d*₂-^{tBu}PN^{tBu}P

¹H NMR (400.13 MHz, C₆D₆)
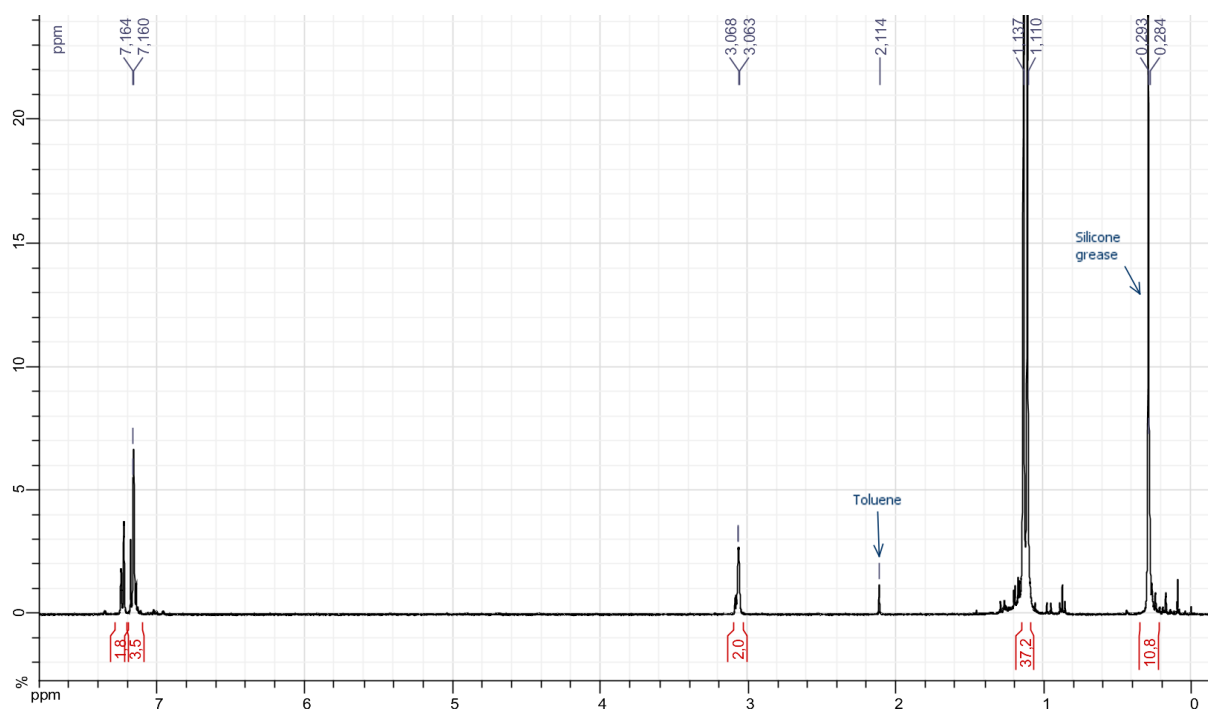
Figure S24. ¹H NMR spectrum of α,α'-*d*₂-^{tBu}PN^{tBu}P in C₆D₆ (residual protio solvent from C₆D₆ at δ 7.16). The presence of silicone grease (δ 0.29) originates from the sample preparation.

¹³C{¹H} NMR (125.77 MHz, C₆D₆)

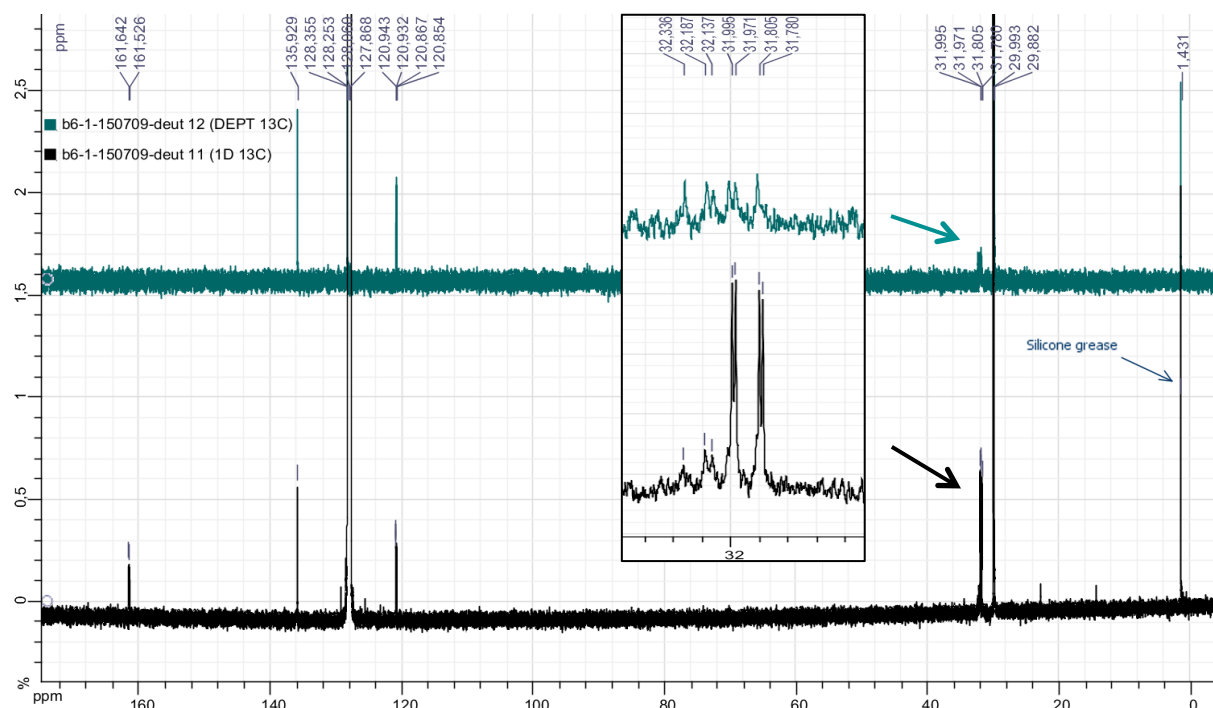**Figure S25**. ¹³C{¹H} (bottom) and ¹³C-DEPT (top) NMR spectra of α,α'-*d*₂-^{tBu}PN^{tBu}P in C₆D₆ (solvent signals at δ 128.06). The presence of silicone grease (δ 1.43) originates from the sample preparation.

³¹P{¹H} NMR (161.98 MHz, C₆D₆)

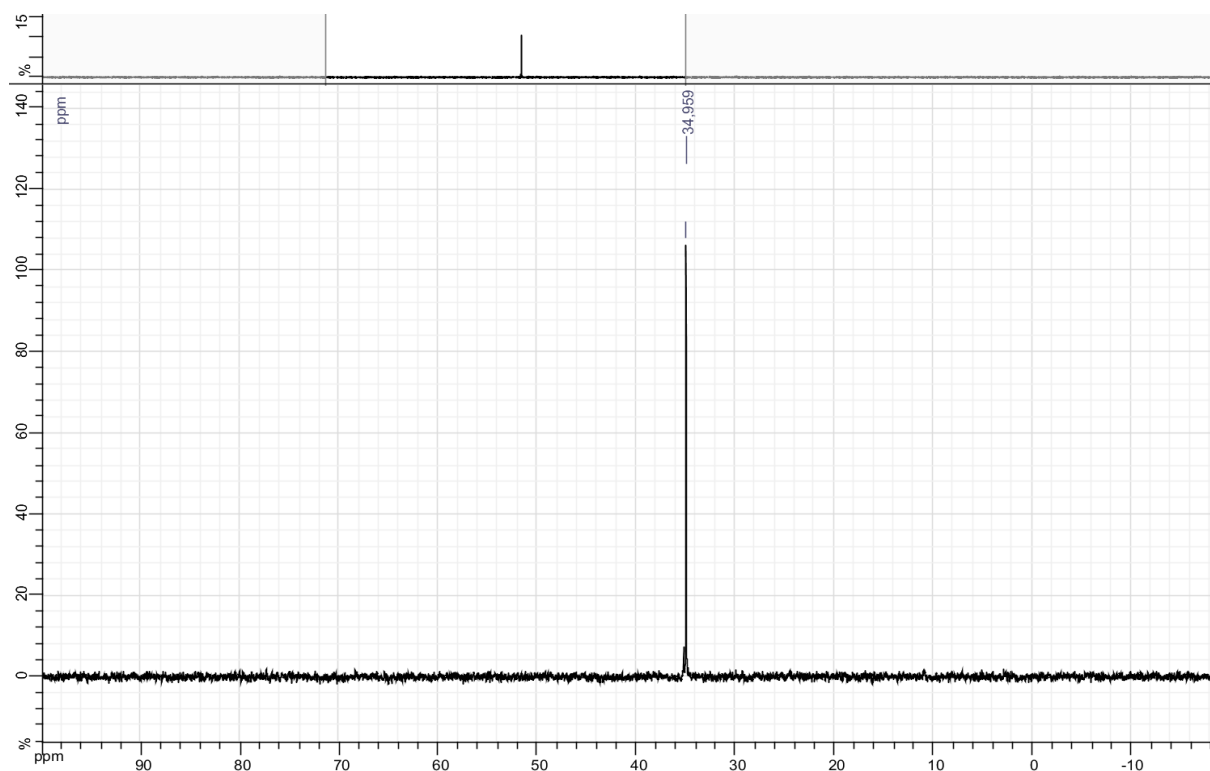**Figure S26.** ³¹P{¹H} NMR spectrum of α,α'-d_2-^{tBu}PN^{tBu}P in C₆D₆.

IV.4. [Cr{Cr(^{tBu}P*N$_a$^{tBu}P*)Cl}₂]
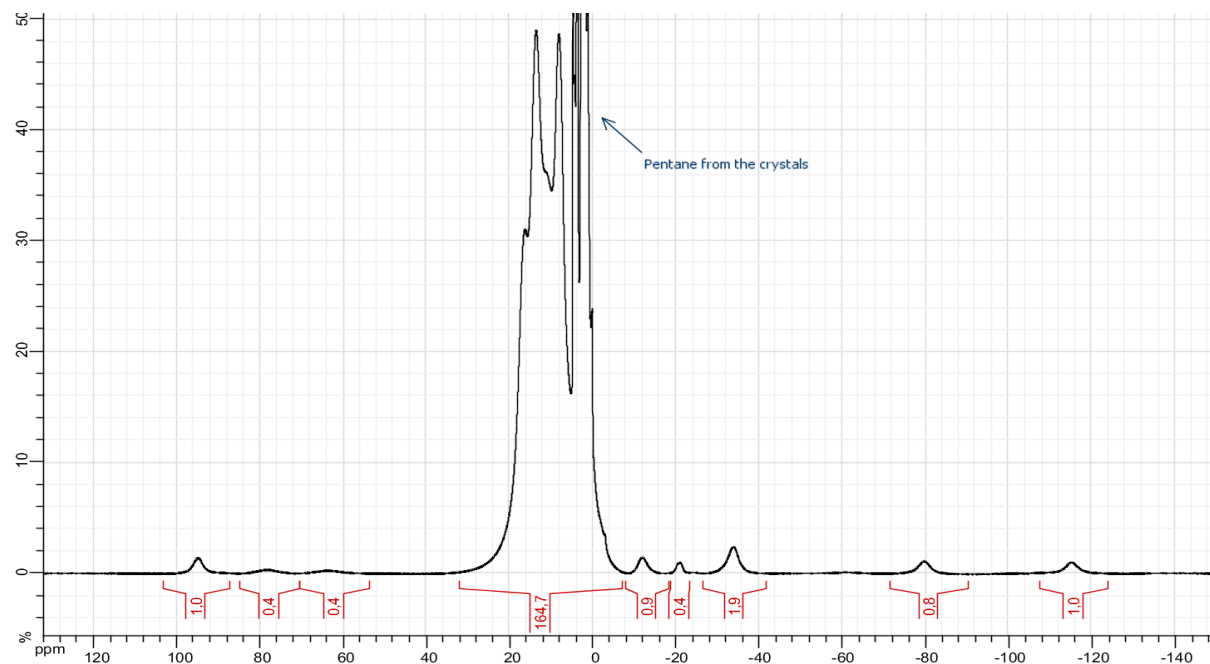
¹H NMR (400.13 MHz, THF-d_8)

Figure S27. ¹H NMR spectrum of paramagnetic **2** in THF-d_8 after baseline correction (spline mode). Signals of the residual protio solvent from THF-d_8 overlap with signals of **2**. Pentane originates from the crystals (one molecule of pentane in the asymmetric unit, *cf.* section II.1).

IV.5. [Zr(tBuP*NatBuP*)Cl2]

The ¹H and ³¹P{¹H} NMR spectra have already been displayed in sections I.6.2 and I.6.3, respectively.

¹³C{¹H} NMR (125.77 MHz, C₆D₆, 298 K)

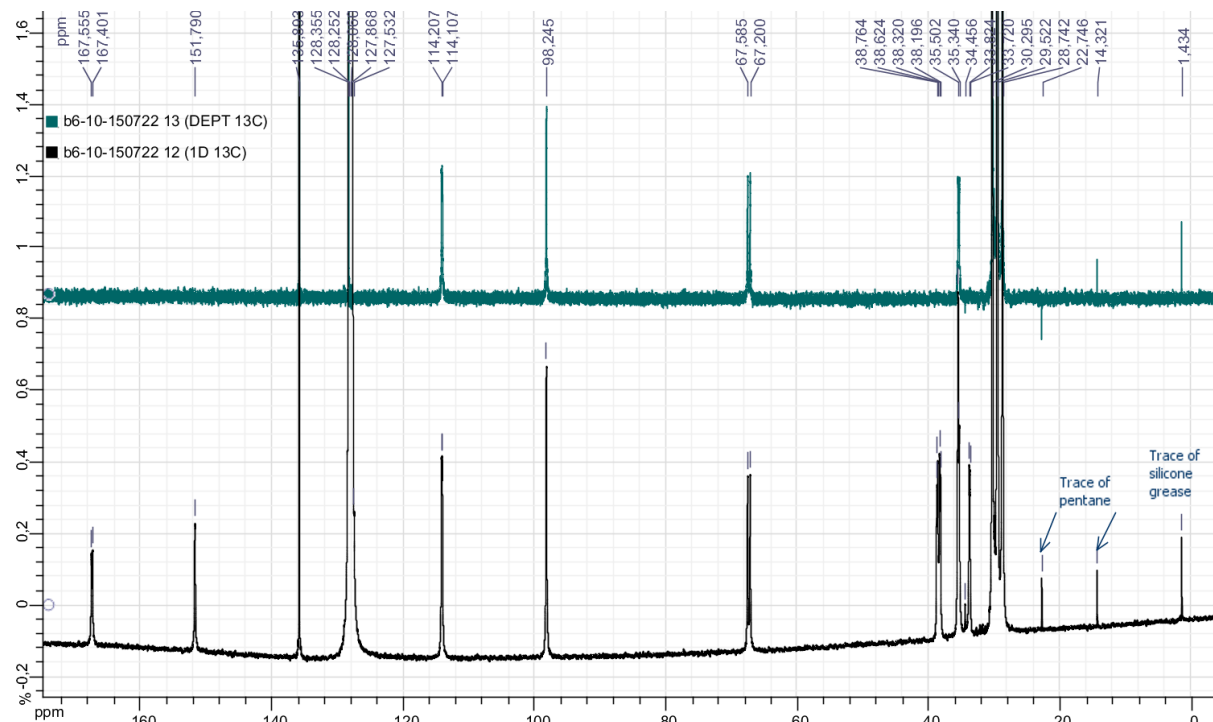**Figure S28**. ¹³C{¹H} (bottom) and ¹³C-DEPT (top) NMR spectra of **3** in C₆D₆ (solvent signals at δ 128.06). Traces of pentane (δ 14.4, 22.7, 34.5) and silicone grease (δ 1.43) are present from the sample preparation.

V. REFERENCES

1. P. J. Bailey, R. A. Coxall, C. M. Dick, S. Fabre, L. C. Henderson, C. Herber, S. T. Liddle, D. Loroño-González, A. Parkin and S. Parsons, *Chem. Eur. J.*, 2003, **9**, 4820.

2. F. M. Chung and A. D. Westland, *Can. J. Chem.*, 1969, **47**, 195.

3. M. Kawatsura and J. F. Hartwig, *Organometallics*, 2001, **20**, 1960.

4. T. Simler, A. A. Danopoulos and P. Braunstein, *Chem. Commun.*, 2015, **51**, 10699.

5. (a) D. F. Evans, *J. Chem. Soc.*, 1959, 2003; (b) E. M. Schubert, *J. Chem. Edu.*, 1992, **69**, 62.

6. D. H. Grant, *J. Chem. Edu.*, 1995, **72**, 39.

7. G. A. Bain and J. F. Berry, *J. Chem. Edu.*, 2008, **85**, 532.

8. H. Günther, ed., *NMR Spectroscopy: Basic Principles, Concepts and Applications in Chemistry (Third Edition)*, Wiley VCH, Weinheim, Germany, 2013.

9. *APEX2*, *SAINT* and *SADABS*, Bruker AXS Inc., Madison, Wisconsin, USA, 2009.

10. (a) G. M. Sheldrick, *Acta Crystallogr., Sect. A*, 2008, **64**, 112; (b) G. M. Sheldrick, *SHELX2013*, University of Göttingen, Germany, 2013.

11. S. Parsons and H. Flack, *Acta Crystallogr., Sect. A*, 2004, **60**, s61.

12. M. J. Frisch, G. W. Trucks, H. B. Schlegel, G. E. Scuseria, M. A. Robb, J. R. Cheeseman, G. Scalmani, V. Barone, B. Mennucci, G. A. Petersson, H. Nakatsuji, M. Caricato, X. Li, H. P. Hratchian, A. F. Izmaylov, J. Bloino, G. Zheng, J. L. Sonnenberg, M. Hada, M. Ehara, K. Toyota, R. Fukuda, J. Hasegawa, M. Ishida, T. Nakajima, Y. Honda, O. Kitao, H. Nakai, T. Vreven, J. A. Montgomery, Jr., J. E. Peralta, F. Ogliaro, M. Bearpark, J. J. Heyd, E. Brothers, K. N. Kudin, V. N. Staroverov, R. Kobayashi, J. Normand, K. Raghavachari, A. Rendell, J. C. Burant, S. S. Iyengar, J. Tomasi, M. Cossi, N. Rega, J. M. Millam, M. Klene, J. E. Knox, J. B. Cross, V. Bakken, C. Adamo, J. Jaramillo, R. Gomperts, R. E. Stratmann, O. Yazyev, A. J. Austin, R. Cammi, C. Pomelli, J. W. Ochterski, R. L. Martin, K. Morokuma, V. G. Zakrzewski, G. A. Voth, P. Salvador, J. J. Dannenberg, S. Dapprich, A. D. Daniels, Ö. Farkas, J. B. Foresman, J. V. Ortiz, J. Cioslowski and D. J. Fox, Gaussian, Inc., Wallingford CT, 2013, Gaussian 09, Revision D.01.

13. Y. Zhao and D. Truhlar, *Theor. Chem. Acc.* 2008, **120**, 215.

14. (a) W. J. Hehre, R. Ditchfield and J. A. Pople, *J. Chem. Phys.* 1972, **56**, 2257; (b) P. C. Hariharan and J. A. Pople, *Theor. Chim. Acta* 1973, **28**, 213; (c) M. M. Francl, W. J. Pietro, W. J. Hehre, J. S. Binkley, M. S. Gordon, D. J. DeFrees and J. A. Pople, *J. Chem. Phys.* 1982, **77**, 3654; (d) T. Clark, J. Chandrasekhar, G. W. Spitznagel and P. v. R. Schleyer, *J. Comput. Chem.* 1983, **4**, 294.

15. (a) D. Andrae, U. Haeussermann, M. Dolg, H. Stoll and H. Preuss, *Theor. Chim. Acta* 1990, **77**, 123; (b) J. M. L. Martin and A. *J.* Sundermann, *Chem. Phys.* 2001, **114**, 3408.

16. (a) M. Bühl and C. van Wüllen, *Chem. Phys. Lett.* 1995, **247**, 63; (b) P. von Ragué Schleyer, C. Maerker, A. Dransfeld, H. Jiao and N. J. R. van Eikema Hommes, *J. Am. Chem. Soc.* 1996, **118**, 6317.

17. K. Wolinski, J. F. Hinton and P. Pulay, *J. Am. Chem. Soc.* 1990, **112**, 8251.

18. (a) E.D. Glendening, C. R. Landis and F. Weinhold, *WIREs Comput. Mol. Sci.* 2012, **2**, 1; (b) C. R. Landis and F. Weinhold, The NBO View of Chemical Bonding, in *The Chemical Bond: Fundamental Aspects of Chemical Bonding*; eds G. Frenking and S. Shaik, Wiley-VCH, Weinheim, 2014.

19. (a) E. D. Glendening, J. K. Badenhoop, A. E. Reed, J. E. Carpenter, J. A. Bohmann, C. M. Morales, C. R. Landis and F. Weinhold, Theoretical Chemistry Institute, University of

Wisconsin, Madison, 2013, NBO 6.0; (b) E. D. Glendening, C. R. Landis and F. Weinhold, *J. Comput. Chem.* 2013, **34**, 1429.

20.   (a) E. D. Glendening and F. Weinhold, *J. Comput. Chem.* 1998, **19**, 595; (b) E. D. Glendening and F. Weinhold, *J. Comput. Chem.* 1998, **19**, 610; (c) E. D. Glendening and F. Weinhold, *J. Comput. Chem.* 1998, **19**, 628.

21.   K. Morokuma, *J. Chem. Phys.* 1971, **55**, 1236.

22.   (a) A. D. Becke, *Phys. Rev. A* 1988, **38**, 3098; (b) J. P. Perdew, *Phys. Rev. B* 1986, **33**, 8822.

23.   (a) T. Ziegler and A. Rauk, *Inorg. Chem.* 1979, **18**, 1558; (b) T. Ziegler and A. Rauk, *Inorg. Chem.* 1979, **18**, 1755.

24.   (a) C. Fonseca Guerra, J. G. Snijders, G. Te Velde and E. J. Baerends, *Theor. Chem. Acc.* 1998, **99**, 391; (b) G. Te Velde, F. M. Bickelhaupt, E. J. Baerends, C. Fonseca Guerra, S. J. A. van Gisbergen, J. G. Snijders and T. Ziegler, *J. Comput. Chem.* 2001, **22**, 931; (c) ADF2013, SCM, Theoretical Chemistry, Vrije Universiteit, Amsterdam, the Netherlands.

25.   E. van Lenthe and E. J. Baerends, *J. Comput. Chem.* 2003, **24**, 1142.

26.   (a) E. van Lenthe, E. J. Baerends and J. G. Snijders, *J. Chem. Phys.* 1994, **101**, 9783; b) E. van Lenthe, A. Ehlers and E. J. Baerends, *J. Chem. Phys.* 1999, **110**, 8943.

27.   M. Mitoraj, A. Michalak and T. Ziegler, *J. Chem. Theory Comput.* 2009, **5**, 962.